New dicynodonts (Therapsida, Anomodontia) from near the Permo–Triassic boundary of Laos: implications for dicynodont survivorship across the Permo–Triassic mass extinction and the paleobiogeography of Southeast Asian Blocks

Journal:	*Journal of Vertebrate Paleontology*
Manuscript ID	JVP-2017-0053.R3
Manuscript Type:	Article
Date Submitted by the Author:	n/a
Complete List of Authors:	Olivier, Chloé; Museum National d'Histoire Naturelle; Sorbonne Université Battail, Bernard; Museum National d'Histoire Naturelle Bourquin, Sylvie; Universite de Rennes 1 Rossignol, Camille; Universidade Federal de Ouro Preto Steyer, Jean-Sébastien; Museum National d'Histoire Naturelle Jalil, Nour-Eddine; Museum National d'Histoire Naturelle; Université Cayi Ayyad
Key Words:	Dicynodontia, Laos, Paleobiogeography, Paleogeography, Permo–Triassic boundary

New dicynodonts (Therapsida, Anomodontia) from near the Permo–Triassic boundary of Laos: implications for dicynodont survivorship across the Permo–Triassic mass extinction and the paleobiogeography of Southeast Asian Blocks

CHLOE OLIVIER, *[,1] BERNARD BATTAIL, [1] SYLVIE BOURQUIN, [2] CAMILLE ROSSIGNOL, [3] J. -SEBASTIEN STEYER, [1] and NOUR-EDDINE JALIL[1,4]

[1] CR2P -Centre de Recherche en Paléontologie –Paris, MNHN –Sorbonne Université –CNRS, 57 rue Cuvier, CP 38, F-75005, Paris, France, chloe.olivier@mnhn.fr, bernard.battail@mnhn.fr, jean-sebastien.steyer@mnhn.fr, nour-eddine.jalil@mnhn.fr;

[2] Univ Rennes, CNRS, Géosciences Rennes, UMR 6118, 35000 Rennes, France, sylvie.bourquin@univ-rennes1.fr;

[3] Universidade de São Paulo, Departamento de Geofísica, Instituto de Astronomia, Geofísica e Ciências Atmosféricas – Rua do Matão, 1226 - Cidade Universitária, Butantã – 05508-090 São Paulo – SP, Brazil

camil.rossignol@gmail.com;

[4] Université Cadi Ayyad, Faculté des Sciences Semlalia, Laboratoire Biodiversité et Dynamique des Ecosystèmes, Boulevard Prince My Abdellah, 40000 Marrakech, Maroc.

*Corresponding author

ABSTRACT—The dicynodonts are an emblematic group of herbivorous therapsids, which survived the Permo–Triassic (P–Tr) crisis. Laotian dicynodonts from stratigraphically constrained beds, recently dated using the U–Pb zircon method, yield new insights into terrestrial faunas of Southeast Asia during latest Permian and the earliest Triassic. Summarily described, they were attributed to the genus *Dicynodon*. We provide a new phylogenetic analysis for Laotian dicynodonts, based on three well-preserved skulls indicating that they belong to two new species: *Counillonia superoculis* gen. et sp. nov. and *Repelinosaurus robustus* gen. et sp. nov. Our phylogenetic analysis within Dicynodontia indicate that 1) *Counillonia* is closely related to some "*Dicynodon*"-grade taxa; and 2) *Repelinosaurus* is a kannemeyeriiform. The phylogenetic affinities of these new Laotian dicynodonts allow discussing the survivorship of multiple lineages (Kannemeyeriiformes and "*Dicynodon*"-grade dicynodontoids) across the P–Tr crisis. The Laotian dicynodonts also shed new light on the paleobiogeography of the Southeast Asia from the late Paleozoic to the early Mesozoic, particularly about the timing of collisions between the Indochina, the South China and the North China blocks. The presence of dicynodonts in Laos most likely in the Early Triassic thus implies that the connection between the Indochina Block and South China Block occurred no later than the latest Permian or earliest Triassic (i.e., when the dicynodonts provide direct evidence for a connection).

INTRODUCTION

The dicynodonts are emblematic Permian and Triassic (P–Tr) therapsids. They constitute an important component of the terrestrial P–Tr fauna and were the dominant herbivores in their ecosystems (Cluver and King, 1983). As such, dicynodonts represent a key group for understanding the impact of the P–Tr crisis on terrestrial environments. Known Early Triassic dicynodont genera include the cosmopolitan speciose *Lystrosaurus*, the small-bodied emydopoids *Myosaurus* from South Africa/Antarctica and *Kombuisia* from Antarctica, and the Chinese kannemeyeriiform *Sungeodon* (Fröbisch et al., 2010; Maisch and Matzke, 2014).

In North China, Liu et al. (2013) used U–Pb zircon method (based on zircon U–Pb sensitive high-resolution ion microprobe [SHRIMP] dating) within the Ermaying and Tongchuan dicynodont-bearing formations (with the kannemeyeriiform genera *Shansiodon* and *Sinokannemeyeria*) and dated them to Early to Middle Triassic. More recently, the higher-resolution chemical abrasion-thermal ionization mass spectrometry (CA–TIMS) dated these formations as Middle Triassic (Anisian–Ladinian) (Liu et al., 2018). Thus, the main kannemeyeriiform radiation seems to have occurred after the beginning of the Triassic, with roughly 40 species known by the Middle Triassic (Fröbisch, 2008).

The first record of dicynodonts in Laos (Southeast Asia) dates back to the 19th century: Counillon (1896) mentioned a poorly-preserved and incomplete skull found in the Purple Claystone Formation (Fm) of the Luang Prabang Basin, northern Laos (Fig. 1A). This specimen was first studied by Repelin (1923), who assigned it to a new species of *Dicynodon*, *D. incisivum*, which he considered to be closely related to *Dicynodon orientalis* from the Panchet Fm of India. Later, Das Gupta (1922)

transferred *D. orientalis* to the genus *Lystrosaurus* and Woodward (1932), followed by Yuan and Young (1934), attributed Counillon's specimen to *Lystrosaurus*. Piveteau (1938) redescribed the specimen and brought the specimen back to *Dicynodon*. Based on this study, Battail (2009) and Kammerer et al. (2011) also favored this taxonomic attribution. Nevertheless this specimen continued to be mentioned as *Lystrosaurus* without further comment (Keyser and Cruickshank, 1979; King, 1988). The Counillon's specimen has unfortunately been lost, preventing further investigations. The illustrations accompanying the original description cannot be interpreted with confidence (Colbert, 1982; Kammerer et al., 2011). The taxon "*Dicynodon incisivum"* should then be considered a nomen dubium (as pointed out by many authors, e.g., Battail, 2009; Fröbisch, 2009; Kammerer *et al.*, 2011).

Between 1993 and 2003, Franco-Laotian expeditions led by P. Taquet (MNHN, Paris, France) collected an abondant dicynodont remains from the Purple Claystone Fm of the Luang Prabang Basin. Among these fossils, three dicynodont skulls (LPB 1993-2, LPB 1993-3, and LPB 1995-9) were tentatively ascribed to the genus *Dicynodon* by Battail (2009). However, no phylogenetic analysis has been performed on these specimens and their relationships with other dicynodonts remain equivocal.

The age of these specimens, collected in the Purple Claystone Fm, has long been a subject of debate. Indeed, this formation was first been attributed to the Early Triassic (Counillon, 1896; Repelin, 1923; Piveteau, 1938), but was later considered to be Late Triassic to Middle Jurassic in age (Saurin, 1962). Based on the dicynodont skulls and their supposed attribution to the genus *Dicynodon* (Battail, 2009), this formation was considered to be late Permian in age (Battail, 2009). Recent geochronological analyses (based on U–Pb detrital zircons dated by Laser Ablation Induction Coupled Plasma Mass Spectroscopy [LA ICPMS]) performed on

volcaniclastic rocks from the Purple Claystone Fm suggest a maximum depositional age of 251.0 ± 1.4 Ma (Table 1) (Rossignol et al., 2016).

This temporal framework thus allows us to document dicynodont survivorship and post-extinction recovery in a P–Tr basin located outside the classic extensively studied Russian (e.g., Benton et al., 2004) and South African ones (e.g., Ward et al., 2005; Smith and Botha-Brink, 2014; Viglietti et al., 2018). The fauna preserved in the Luang Prabang Basin also offers new evidence concerning the paleobiogeography of dicynodonts.

Here, we provide detailed description of the three Laotian skulls (LPB 1993-2, LPB 1993-3, and LPB 1995-9), which represent two new taxa. Phylogenetic analysis is then performed to test the relationships of these new taxa within Dicynodontia.

Institutional Abbreviations—BP, Evolutionary Studies Institute (formerly known as the Bernard Price Institute for Palaeontological Research and the Institute for Human Evolution), Johannesburg, South Africa; **LPB**, Laotian specimens found in the Luang Prabang Basin currently in the Savannakhet Dinosaur Museum, Savannakhet, Laos; **MCZ**, Museum of Comparative Zoology, Harvard University, Cambridge, Massachusetts, USA; **NHMUK**, Natural History Museum, London, UK.

Anatomical Abbreviations— aPt, anterior ramus of the pterygoid; **Bo**, basioccipital; **Ch**, choana; **EcPt**, ectopterygoid; **Eo**, exoccipital; **EpiPt**, epipterygoid; **Fm**, foramen magnum; **Fr**, frontal; **Ip**, interparietal; **Ipv**, interpterygoid vacuity; **Ju**, jugal; **La**, lacrimal; **Laf**, lacrimal foramen; **Lbf**, labial fossa; **mPt**, median plate of the pterygoid; **Mx**, maxilla; **Na**, nasal; **Oct**, occipital tuber; **Opt**, opisthotic; **Pa**, parietal; **Pal**, palatine; **Pant**, pila antotica; **Pbs**, parabasisphenoid; **Pi**, pineal foramen; **Pm**, premaxilla; **Po**, postorbital; **Pp**, preparietal; **PrF**, prefrontal; **Q**, quadrate; **Qj**, quadratojugal; **qPt**, quadrate ramus of the pterygoid; **Smx**, septomaxillae; **So**,

supraoccipital; **Sq**, squamosal; **T**, tusk; **Tpf**, postemporal fenestra; **Vo**, vomer; **Va**, vagus nerve aperture.

GEOLOGICAL SETTING

The Luang Prabang Basin, located in the Indochina Block (Fig. 1A), was originally studied by Counillon (1896) and consists of an asymmetric NE–SW (Northeast–Southwest) syncline with NE–SW thrusts separating the Purple Claystone Fm and the Limestone and Sandstone Fm to the North from younger formations to the South (Fig. 1B; Blanchard et al., 2013).

The Limestone and Sandstone Fm is made up of shallow marine deposits, dated to the late Changhsingian on the basis of its ammonoid remains (Blanchard et al., 2013). These marine deposits are overlain by black claystone layers, containing a typical Cathaysian flora (Bercovici et al., 2012).

The Limestone and Sandstone Fm is overlain by the Purple Claystone Fm, from which various fossil remains have been excavated (dicynodonts and a chroniosuchian; Steyer, 2009; Arbez et al., 2018). The Purple Claystone Fm is mainly composed of homogeneous silty-claystones, silts, and more rarely clays (Bercovici et al., 2012). The formation also comprises volcaniclastic siltstones and sandstones, with millimetric to centimetric rounded and highly-weathered volcaniclasts (up to about 20 vol.%). These volcaniclasts exhibit a variety of volcanic textures (microlithic, trachytic, porphyritic), and are sometimes embedded within lithic fragments, attesting to multiple reworking events for these volcaniclasts (Bercovici et al., 2012; Blanchard et al., 2013). The Purple Claystone Fm also contains subordinate amounts of coarser deposits, including sandstone and conglomeratic facies with 3D megaripples typical

of braided river deposits. Conglomeratic levels consist of rounded pebbles of highly fossiliferous limestones (foraminifers, corals, bryozoans), sub-angular to rounded pebbles of volcanic rocks, black cherts, red quartzites, red sandstones, and siltstones. Paleosols, sometimes exhibiting vertical root traces, are developed within this formation (Bercovici et al., 2012). The sedimentary facies association indicates braided river depositional environments, evolving vertically to alluvial plain environments, probably including ponds (Bercovici et al., 2012).

Three samples from the Purple Claystone Fm, including one collected at the dicynodont site (Fig. 1C), were dated using U–Pb geochronology on detrital zircon (Rossignol et al., 2016). The sample collected at the dicynodont fossil site yielded a maximum depositional age of 252.0 ± 2.6 Ma, whereas the other volcaniclastic samples collected in the same formation yield maximum depositional ages of 251.0 ± 1.4 Ma and 300.5 ± 3.7 Ma (Table 1). The various volcaniclastic textures, their roundness, the relatively low volcaniclast content (below 20%) implying an important and protracted mixing with other detrital particles, as well as the fact that some of the volcaniclasts underwent at least two sedimentary cycles (Bercovici et al., 2012; Blanchard et al., 2013), suggest that these dates, obtained from zircon grains interpreted as being detrital in origin, represent maximum depositional ages. The actual age of deposition of the Purple Claystone Fm is therefore likely to be younger. Both youngest maximum depositional ages (i.e., 252.0 ± 2.6 Ma and 251.0 ± 1.4 Ma) encompass the P–Tr boundary (251.902 ± 0.024 Ma; Burgess et al., 2014) within uncertainties. The consideration of a late Permian age, potentially plausible, would nonetheless imply that the reworking of the zircon grains took place within an unlikely brief time span. Given the age of the overlying formation (224.9 ± 1.0 Ma; Blanchard et al., 2013), an age up to the Carnian could be proposed as the theoretical upper

age limit for the Purple Claystone Fm. However, the occurrence of a regional Middle Triassic unconformity (e.g., Racey, 2009), probably superimposed onto the reverse fault separating the Purple Claystone Fm from other sedimentary units to the SE (Fig. 1B), reduces the likely time span for the deposition of the Purple Claystone Fm. As a consequence, an Early Triassic age for the Purple Claystone Fm and its enclosed fossils is considered as the most likely.

SYSTEMATIC PALEONTOLOGY

The interpretation of the cranial bone contacts is based either on direct observations of the scarce preserved sutures or on relief differences. When possible, some sutures were deduced from the contacts between the surrounding bones.

THERAPSIDA Broom, 1905

ANOMODONTIA Owen, 1860

DICYNODONTIA Owen, 1860

DICYNODONTOIDEA Olson, 1944

COUNILLONIA gen. nov.

Type Species—*Counillonia superoculis* gen. et sp. nov., monotypic.

Etymology—In honour of the French geologist Jean-Baptiste-Henri Counillon, member of the Pavie Missions, who was the first to mention the occurrence of dicynodonts in the Luang Prabang Basin (Counillon, 1896; see Steyer, 2009 for a biography).

Diagnosis—See diagnosis of the type species.

COUNILLONIA SUPEROCULIS gen. et sp. nov.

(Fig. 2)

Etymology—From the Latin oculis (dative plural of oculus, eye) and super (upwards), referring to its largely dorsally opening orbits due to an especially narrow interorbital bar.

Holotype—LPB 1993-3, a skull without mandible (basal length: 16.02 cm, maximum width: 13.41 cm). The posterior side of the left orbit, the quadrates, and the stapes are missing. The dorsal surfaces of the premaxilla, nasals, prefrontals, and frontals are partially eroded. The preparietal, prootic, and epipterygoid are poorly preserved.

Geographic Distribution and Stratigraphic Range—The specimen LPB 1993-3 (19° 55’ 59’’ N, E 102° 07’ 41’’ E) was discovered in the Purple Claystone Fm, Luang Prabang Basin (Laos). This formation was initially attributed to the Early Triassic by Counillon (1896) then to the late Permian by Battail (2009). Recent geochronological (U–Pb on detrital zircon; Rossignol et al., 2016) analyses suggest a maximum depositional age of 251.0 ± 1.4 Ma (see “Geological setting” above).

Diagnosis—Medium-sized dicynodontoid characterized by the unique combination of the following character states: a reduced premaxillary secondary palate; a naso-frontal suture with a distinct posterior process; a narrow intertemporal bar; a reduced temporal fenestra; a pineal foramen located in the posterior quarter of the dorsal skull length; an acute angle of the squamosal wings in lateral view; zygomatic squamosal rami posteriorly inserted at mid-height of the occiput; a relatively large median pterygoid plate; high-angled posterior pterygoid rami; anterior

rami of the pterygoids ventrally highly expanded; a long interpterygoid vacuity; no intertuberal ridge; distinct exoccipital and basioccipital contributions to the occipital condyle; a very sharp and posteriorly directed lateral edge of the paroccipital process, which is distinctly offset from the surface of the occipital plate. The naso-frontal suture with a distinct posterior process distinguishes *Counillonia* from the Laotian *Repelinosaurus* and "*Dicynodon*"-grade taxa. Further distinguished from closely related "*Dicynodon*"-grade taxa by a pineal foramen located far posteriorly and a large median pterygoid plate. Further distinguished from *Repelinosaurus* by an anteriorly-directed caniniform process, a narrow interorbital bar, a triangular occiput, and zygomatic squamosal rami posteriorly inserted at mid-height of the occiput.

Description—The skull is slender and short, with a short preorbital region and a narrow snout. In dorsal view, the skull is relatively broad with zygomatic arches laterally expanded. The combination of the laterally bowed zygomatic arches and narrow interorbital result in notably dorsally-directed orbits (Fig. 2A). The surfaces of the premaxilla, the maxillae, the nasals, the frontals, and the postorbitals are weathered. Because of this, the mid-nasal, naso-premaxillary, preparieto-frontal, and postorbito-parietal sutures are not visible (Fig. 2A). The absence of visible sutural contacts in the weathered narial region precludes determination of the possible presence of the septomaxillae (Fig. 2B). It is thus not clear whether the septomaxillae form part of the ventrolateral margin of the nares, which seem to be formed only by the premaxilla anteriorly, the nasals dorsolaterally, and the maxillae ventrolaterally. In addition, the bone contacts cannot be discerned on the occiput, nor along the medial partition of the temporal and orbital fossae (Fig. 2B, D).

The short premaxilla is fused and forms the anterior portion of the snout that constricts and ends in a squared tip. The tip of the snout shows weak ventral

curvature in anterior view (not figured here) as in *Tropidostoma* and *Aulacephalodon* (Kammerer and Smith, 2017). However, this curvature and possible ridges or rugosities cannot be confirmed due to the poor preservation of the dorsal surface of the premaxilla. The premaxilla contributes to the external anterior edge of the naris. The large narial opening is situated near the anterior and ventral edges of the snout, and contributes to more than a third of the surface of the snout (Fig. 2B). The external ventral margin of the naris is visible in dorsal view (Fig. 2A). The premaxilla contacts the nasals posterodorsally and the maxilla posterolaterally at the level of the anterior third of the nares. In ventral view, the premaxilla bears two thin parallel longitudinal ridges (the anterior palatal ridges) that surround a wide, median longitudinal depression and extend beyond the anterior third of the palatal surface (Fig. 2C). This depression turns posteriorly into a sharp crest (the median palatal ridge), which extends to the vomer posteriorly and is flanked on either side by flat depressions. The height of this longitudinal ridge increases posteriorly. On the palatal surface, the premaxilla contacts the maxillae laterally. The absence of visible sutures between the premaxilla and the palatines yields no information about a potential contact (Fig. 2C). The nasals bear a median, rugose and well-developed boss, which extends onto the bones bordered by two wide elongated depressions that broaden posteriorly and terminate on the frontals (Fig. 2A). However, as mentioned above, the poor preservation of the snout surface precludes firm conclusions to be reached about the original external relief of the nasals. The nasals are surrounded by the frontals and the prefrontals posteriorly, the premaxilla anteriorly, and the maxillae and lacrimals laterally (Fig. 2A, B).

The prefrontals form the anterodorsal edge of the orbits. On the external surface of the skull, they contact the frontals medially, the lacrimals laterally, and the nasals

anteriorly (Fig. 2A). A single rugose boss is visible on each prefrontal. However, as already noted for the nasals, there is no reliable information about the original relief of the bones due to the poor preservation of their external surfaces.

The frontals form the major part of the skull roof (Fig. 2A). The sutures of the frontals can be discerned along their contact with the postorbitals, the prefrontals, and the nasals, as well as the interfrontal one (Fig. 2A). The external surface of the skull roof is poorly preserved; the presence of postfrontals cannot be confirmed in LPB 1993-3. The naso-frontal suture has a distinct posterior process. The dorsal margin of the orbits seems to be largely made up of the frontals. Apart from a small chip of bone missing on the right dorsal margin of the orbit, the rest of its margin appears to be preserved, with a symmetry of the lateral margins of the orbits and continuous lateral borders. The interorbital region is broader than the intertemporal bar (Fig. 2A).

The preparietal is strongly weathered and its anterior part is missing. However, its posterior region displays a small bulge anterior to the pineal foramen, the relief possibly being due to its poor preservation (Fig. 2A). The contact between the preparietal and the nearby bone (the postorbitals, the frontals, and the preparietal) cannot be determined.

The dorsal exposure of the parietals is limited to a midline groove between the posterior postorbital processes (Fig. 2A). The parietals then contact the postorbitals laterally and dorsally. External sutural contacts between the parietals and the frontals are invisible due to the poor preservation of the preparietal and the eroded external surface of the skull roof. The pineal foramen is surrounded by the parietals posteriorly, and by the preparietal anteriorly. The oval pineal foramen, with a length of 1.36 cm and a width of 0.96 cm (Table 2), has its long axis perpendicular to the axis

of the intertemporal bar. It is located in the posterior quarter of the skull roof (continuous character 7, Appendix 1).

The slender postorbitals have lateral and posterior processes. The posterior postorbital process merges along the intertemporal bar, posterior to the pineal foramen (Fig. 2A). The temporal portion of the postorbitals appears to be oblique with a dorsolateral orientation. However, the poor preservation of the external surface of the postorbital does not allow confirmation of this orientation with certainty. The posterior postorbital region is thinner than the preorbital one (Fig. 2A). The postorbitals extend along almost the entire intertemporal bar, bordering the temporal fossae medially and anteriorly (Fig. 2A). They thus constitute the posterior margin of the orbits. On their external surface, the posterior postorbital processes contact mainly the squamosals and to a lesser degree the interparietal posteriorly, the parietals medially, and the frontals anteriorly. As mentioned above, no reliable information can be provided on the contact between the postorbitals, the frontals, and the preparietal. The lateral postorbital processes have a sutural contact with the jugals anteroventrally and the zygomatic squamosal processes posteroventrally (Fig. 2B).

The maxillae form the largest part of the lateral surface of the snout. They contact the premaxilla anteriorly, the lacrimals and the nasals dorsally (Fig. 2B). The maxillo-nasal suture lies on the dorsal edge of the nares. There is no sutural contact between the maxillae and the prefrontals due to the anterior expansion of the lacrimals that contacts the nasals. The maxillary zygomatic process is posteriorly pointed, and contacts the squamosal posteriorly and the jugal dorsally (Fig. 2B). The maxillae bear short caniniform processes housing tusks. The dorsal edge of the erupted portion of the tusk is anterior to the anterior edge of the orbits. The caniniform processes and

the tusks face anteriorly. The tusks have a sub-circular basal section (Fig. 2C; Table 2). On the ventral surface, no maxillary teeth are observed except the tusks (Fig. 2C). The maxillae contact the anterior rami of the pterygoids and the ectopterygoids posteriorly, and the jugals and the squamosals laterally. No boundaries are visible in front of the palatines, and nothing can be confirmed about the extension of medial maxillary processes posterior to the premaxilla. In *Lystrosaurus* (e.g., Cluver, 1971) and *Kannemeyeria lophorhinus* (e.g., the holotype, BP/1/3638, and the specimen formerly referred to *Rechnisaurus cristarhynchus*, NHMUK R11955 [Renaut et al., 2003; C. Olivier, pers. obs., 2018]), these processes exclude the contact between the premaxilla and the palatines. A depression lies on the suture between the maxillae and the pterygoids (Fig. 2B). A broad labial fossa opens posterior to the tusk (Fig. 2C). Its boundaries cannot be discerned; however, it is usually surrounded by the maxillae ventrally, the jugals dorsolaterally, and the palatines medially (e.g., Cluver 1971). It is therefore not certain whether *Counillonia* has a true labial fossa (circumscribed by the maxillae, the palatines, and the jugals) or a comparable structure to the foramen in dicynodonts such as *Diictodon*, *Endothiodon* or *Dicynodontoides* (e.g., Angielczyk and Kurkin, 2003).

The lacrimals are relatively triangular in lateral view (Fig. 2B). They contact the nasals and prefrontals dorsally, the maxillae ventrally, and the jugals posteriorly. Their anterior well-developed expansions exclude a maxillo-prefrontal sutural contact. Their sutures within the orbits are not visible. The lacrimals constitute the anterior margin of the orbits with the jugals anteroventrally and the prefrontals anterodorsally (Fig. 2B). Within the orbit, each lacrimal is perforated by a single foramen (Fig. 2A).

The jugals are longitudinally elongated and form the ventral edge of the orbits (Fig. 2B). However, their expansion within the orbits and their natural limits cannot be

discerned due to the absence of visible sutures, as noted above. Visible sutures on the lateral side of the skull show a long scarf joint with the maxillae ventrally, a jugal posterior process contacting the postorbitals posteriorly, and a small contact with the zygomatic squamosal processes ventroposteriorly and the lacrimals anterodorsally (Fig. 2B).

The squamosals are triradiate with zygomatic, temporal, and quadrate rami. The zygomatic ramus shapes the posterior region of the zygomatic arch (Fig. 2B). In dorsal view (Fig. 2A), it widens posteriorly into a wing-shaped structure without a folded edge. It becomes narrow in the pointed anterior region, without dorsoventral expansion posterior to the postorbital bar (Fig. 2B). The squamosal zygomatic processes contact the jugals, the postorbitals, and the maxillae anteriorly (Fig. 2B). They circumscribe laterally and partly posteriorly the temporal fossae. The zygomatic squamosal rami show a relatively ventral insertion on the back of the skull, at mid-height on the occiput (Fig. 2D). On the lateral side, they do not reach the dorsal region of the occiput. The temporal processes delimit the temporal fossae posteromedially. On their external surface, they contact the postorbitals dorsally. On their occipital side, no contact between bones is visible (Fig. 2D). The absence of the limits of the tabulars does not allow us to determine whether the squamosals are separated from supraoccipitals by the tabulars. The steep angle between the temporal and zygomatic processes of the squamosal slightly exceeds 90° (Fig. 2D). The wide lateral extensions of the squamosal make an angle of less than 90° with the occipital side. A part of the lateral edge of the occiput is thus hidden. The squamosals extend posterior to the occipital condyle (Fig. 2C).

The lateral surface of the braincase is strongly eroded but bone structures can be noted. Although the sutural contacts of the prootics are not visible, the basal part of

the left pila antotica (not figured here) is preserved. Only the dorsal region of the long and narrow epipterygoids, which contacts the ventral process of the parietals, is preserved. A strong anteroventral depression in the squamosals indicates the connection with the missing quadrates (Fig. 2B).

The vomer displays a tuberosity turning into a vertical blade, which narrows posteriorly and separates the two choanae (Fig. 2C). The width of the median blade is constant along its length. The vomer contacts the premaxilla anteriorly and the pterygoids posteriorly. It forms the anterior margin of an elongated and ovoid interpterygoid vacuity (Fig. 2C).

The palatines border the choanae anterolaterally. The anterior palatine expansions form rugose and textured pads indicating a keratinized covering (Fig. 2C). They narrow posteriorly to form relatively smooth processes. The palatines contact the anterior rami of the pterygoids along their entire lateral scarf joint and are anteriorly bordered by the maxillae. However, as mentioned above, due to the uncertainties about their anterior sutural contact, it is not clear whether they contact the premaxilla. A lateral palatine foramen is present alongside each anterior expanded pad (Fig. 2C).

Each pterygoid has an anterior ramus and a posterior (or quadrate) ramus. A single median plate connects the two bones and links the four rami. The pterygoids contact the secondary palate and the basicranium (Fig. 2C). Their ventral projections extend strongly anteroventrally, such that they form an anterior depression with the maxillae (Fig. 2B). These anterior pterygoid keels extend along most of the length of the anterior rami. Nevertheless, this extension cannot be precisely measured because the sutures are not visible laterally (Fig. 2B). The anterior rami of the pterygoids merge from the median plate, posterior to the interpterygoid vacuity. The interpterygoid vacuity is thus bordered by the pterygoids posteriorly and the vomer

anteriorly. The posterior margin of the vacuity rises flush with the median plate of the pterygoids. The ventral surface of the narrow median plate bears a thin crista oesophagea (Fig. 2C). The median plate of the pterygoids contacts the parabasisphenoid posteriorly and the vomer anteriorly. In addition, a possible contribution of the parabasisphenoid to the interpterygoid vacuity cannot be proved. Two posterior rami of the pterygoids contact the squamosal fossa posteriorly and probably the medial condyles of the quadrates laterally.

Despite the absence of visible sutural contacts on the lateral side of the skull, the presence of the ectopterygoids is indicated by a variation in bone texture on the lateral border of the anterior rami of the pterygoids (Fig. 2B). The ectopterygoids have a slender leaf shape and expand laterally along the anterior rami of the pterygoids. They do not expand posterior to the palatines in palatal view (Fig. 2C).

The crista oesophagea continues onto the parabasisphenoid and then diverges posteriorly to form the ridges leading to the basitubera (Fig. 2C). The contribution of the parabasisphenoid to the fenestra ovalis of the tubera is considerably restricted in comparison with the basioccipital. The stapedial facet is ventrolaterally directed and its narrow margin mostly extends anteroposteriorly. The paired carotid canals, located in the anterior region of the parabasisphenoid in many dicynodonts (e.g., Maisch, 2002; Surkov and Benton, 2004), are not visible here. No intertuberal ridge is visible. The basioccipital extends onto the occipital plate and with the exoccipitals forms a tripartite occipital condyle (Fig. 2D). The exoccipitals and the basioccipital appear not to be fused in the condyle. A circular central depression is located between the three occipital sub-condyles. Medially, the exoccipitals border the aperture of the vagus nerves (Dutuit, 1988).

The contacts between the interparietal and the other bones, forming the occipital side and the posterior region of the skull roof, cannot be discerned (Fig. 2D). Despite the eroded surface of the posterior postorbital processes, the interparietal does not seem to contribute to the skull roof (Fig. 2A).

The occiput is triangular in posterior view (Fig. 2D). Although sutures are not clearly preserved, the overall similarity of the occiputs of the *Counillonia* type specimens to those of other dicynodonts (Cluver, 1971: *Lystrosaurus*; Cluver & Hotton III, 1981: *Dicynodon* and *Diictodon*) suggests that they shared a similar construction of the occiput. The teardrop-shaped foramen magnum may be laterally bordered by the exoccipitals, which overhang the basioccipital as in other dicynodonts. They would also contact the supraoccipital dorsally, the opisthotics laterally, and the basioccipital ventrally. A central depression on the supraoccipitals overhangs the foramen magnum and is dorsally bordered by a weak transverse nuchal crest, which extends upwards towards the interparietal. The extent of the tabulars cannot be determined. The broad oval post-temporal fenestrae are located dorsal to the level of the occipital condyle, at the transverse level of the mid-height of the foramen magnum (Fig. 2D). They are oriented in the ventromedial-dorsolateral axis and would be delimited by the squamosal laterally, the supraoccipital dorsomedially, and the opisthotic ventromedially as in most dicynodonts. An oblique ridge on the supraoccipital extends over the fenestra. This ridge continues, below the fenestra, on the opisthotics and terminates in a sharp tuberosity.

KANNEMEYERIIFORMES Maisch, 2001

REPELINOSAURUS gen. nov.

Type Species—*Repelinosaurus robustus* gen. et sp. nov., monotypic.

Etymology— In honour of the French geologist Joseph Répelin, member of the Pavie Missions, who described and named Counillon's dicynodont skull "*Dicynodon incisivum*" (Répelin, 1923; see Steyer, 2009 for a biography). Also from the latinized Greek saurus (a lizard) often used for non-mammalian synapsids, colloquially known as 'mammal-like reptiles'.

Diagnosis—See diagnosis of the type species

REPELINOSAURUS ROBUSTUS gen. et sp. nov.

(Figs. 3–5)

Etymology—From the Latin robustus (robust) referring to its robust cranial appearance.

Holotype—LPB 1993-2, a partial skull without mandible (basal length: 19 cm). The left postorbital bar, the zygomatic arch, the dorsolateral wing of the squamosal, the left quadratojugals, the quadrates, more than half of the left part of the occipital side, the external portion of the tusks, and the stapes are missing. The palatal surface is strongly eroded: most of the sutures cannot be made out and some bones are poorly preserved or are missing.

Referred Material—LPB 1995-9 is a skull (basal length: 15.72 cm) lacking the mandible, the right quadrate ramus of the pterygoid, the left stapes, the quadrates, and the left quadratojugal. The right stapes and the epipterygoids are poorly preserved. The specimen was subjected to lateral compression. However, the left orbit seems to have maintained its original shape.

Geographic Distribution and Stratigraphic Range—Same as for *Counillonia* (see above), LPB 1993-2 (19° 55' 59'' N, 102° 07' 41'' E) and LPB 1995-9 (19° 55' 16'' N, 102° 06' 27'' E) were collected in the Purple Claystone Fm, Luang Prabang Basin (Laos).

Diagnosis—Medium-sized dicynodontoid characterized by the unique combination of the following character states: a reduced preorbital region; a notch on the dorsal edge of the narial opening; nasal bosses present as a median swelling with a continuous posterior margin; a straight fronto-nasal suture; parietals exposed in midline groove; a relatively flat temporal portion of the postorbital, so that most of the exterior surface of the bone faces dorsally; a vertical caniniform process; high insertion of the zygomatic squamosal rami on the occiput posteriorly. Distinguished from all dicynodontoids by a very small preorbital region. Further distinguished from all kannemeyeriiforms by a median nasal swelling with a continuous posterior margin and a flat temporal portion of the postorbital. Further distinguished from the Laotian *Counillonia* by a wide interorbital bar, a straight fronto-nasal suture, a vertical caniniform process, a rectangular occiput, and a high insertion of the zygomatic squamosal rami on the occiput posteriorly.

Remarks—Some differences distinguish LPB 1993-2 and LPB 1995-9 such as (1) the position of the pineal foramen on the skull roof more posterior in LPB 1993-2 (continuous character 6, Appendix 1); (2) a higher angulation between the occiput and the palate in LPB 1993-2 (continuous character 13, Appendix 1); (3) a relatively flat palatal surface of the premaxilla in LPB 1993-2 or with marked depressions on either side of the median crest in LPB 1995-9 (discrete character 29, Appendix 1); (4) a sutural contact between the maxillae and the prefrontals present in LPB 1995-9 and absent in LPB 1993-2 (discrete character 49, Appendix 1); (5) a preparietal

depressed in LPB 1993-2 or flush with the skull roof in LPB 1995-9 (discrete character 68, Appendix 1); (6) a bigger pineal foramen in LPB 1995-9 (Table 2); (7) a tusk basal section compressed mediolaterally in LPB 1995-9 and anteroposteriorly in LPB 1993-2 (Table 2); and (8) more-developed ornamentation on the frontals in LPB 1993-2. However, each character state variation noted could be due to taphonomic deformation, ontogeny, sexual dimorphism or other intraspecific variability (discussed below). Moreover, LPB 1995-9 and LPB 1993-2 were found in the same geological formation, suggesting conspecificity.

Description—The skulls are narrow and robust with a wide and short snout that narrows slightly anteriorly, and terminates in a squared tip. *Repelinosaurus* has a wider interorbital region (Figs. 3A; 4A) than *Counillonia* (Fig. 2A). The orbits are thus open mainly laterally. The dorsal surfaces of the premaxilla, maxillae, and nasals of LPB 1995-9 are weathered, but the preservation of these surfaces in LPB 1993-2 displays strong rugosities on the snout (Figs. 3A; 4A). Nevertheless, the naso-premaxillary and the mid-nasal sutures cannot be traced in LPB 1993-2. The septomaxilla is well preserved in LPB 1995-9 unlike LPB 1993-2 where the poor preservation of the naris does not yield information about this bone (Figs. 3B; 4B; 5). Sutures are not visible on the occiput of either specimen, except for the connection of the right quadrate in LPB 1995-9. The scarf joints also cannot be discerned on the medial portion of the temporal and orbital fossae, but the dorsal head of the epipterygoid and the basal region of the pila antotica are preserved in LPB 1995-9 (Fig. 4B). The palatal surface of LPB 1993-2 is poorly preserved; few sutures are thus visible.

As mentioned above, lots of pits and strong rugosities mark the dorsal surface of the premaxilla in LPB 1993-2 and extend onto the nasals before stopping abruptly at

the naso-prefrontal and naso-frontal sutures (Fig. 3A). These rugosities are thought to indicate a keratinized covering (e.g., Angielczyk et al., 2018). The premaxilla contributes to the external anterior edge of the nares. In lateral view, the well-developed nares of both LPB 1995-9 and 1993-2 represent more than half of the length of the snout (Figs. 3B; 4B). Their ventral edges are close to the ventral border of the snout. The premaxilla is toothless and anteriorly bears two short parallel longitudinal ridges, which are separated by a shallow depression and overlie the anterior quarter of the premaxilla (Figs. 3C; 4C). An anterior rounded pit of medium size in LPB 1993-2, visible posterior to the premaxillary longitudinal crest, could be of taphonomic origin (Fig. 3C). Posterior to this depression, a sharp median ridge extends onto two-thirds of the premaxilla. In LPB 1993-2, the premaxilla is relatively flat. However, this median ridge is surrounded by two depressions, which deepen in the posterior region of the secondary palate in LPB 1995-9. These depressions may be caused by taphonomic lateral compression (discussed below). The premaxilla contacts the nasals posterodorsally and the maxillae posterolaterally at the level of the anterior third of the nares in LPB 1995-9 (Figs. 3B; 4B). However, the sutures of the premaxilla with the nasals and maxillae are not visible in LPB 1993-2. In both LPB 1995-9 and 1993-2, on the palatal surface, the premaxilla contacts the maxillae and their caniniform processes laterally. However, the suture between the premaxilla, maxillae, and palatines are not clearly preserved (Figs. 3C; 4C).

The well-developed nasal bosses terminate laterally in a posterodorsal notch at the dorsal edge of the nares, and are separated from the frontals and prefrontals by a shallow depression (Figs. 3B; 4B). The notch on the posterodorsal edge of the naris is formed by a thick expansion of the nasal bosses, which hides the external ventral narial edge in dorsal view. The bosses form a median swelling that is more marked in

LPB 1993-2 than in LPB 1995-9 (Figs. 3B; 4B). The nasals are bordered by the frontals and the prefrontals posteriorly, the premaxilla anteriorly, and the maxillae laterally. However, the nasals do not contact the lacrimals in LPB 1995-9, in contrast to LPB 1993-2 (Figs. 3B; 4B; 5).

The prefrontals form the edge of the orbits with the lacrimals anteriorly, the jugals ventrally, the postorbitals posteriorly, and the frontals dorsally (Figs. 3A, B; 4A, B). As for the nasals, the prefrontal extension is broader in dorsal than in lateral view. The prefrontals bear a weak boss, distinct from the nasals. The prefrontals contact the maxillae ventrally in LPB 1995-9 (Figs. 4B; 5).

The interorbital region of *Repelinosaurus* (Figs. 3A; 4A) is clearly wider than that of *Counillonia* (Fig. 2A). In *Repelinosaurus*, it is mainly formed by the frontals constituting the dorsal margin of the orbits, which rise slightly laterally. In addition, as mentioned above, the prefrontals bear bosses in both specimens. The interorbital region obscures the orbits in dorsal view, their orientation is thus mainly lateral while it is dorsolateral in *Counillonia*. In LPB 1993-2, the frontals are separated by a sharp median ridge bordered by two deep depressions (Fig. 3A). In LPB 1995-9 the preparietal, the parietals, and the posterior region of the frontals show a depression. The frontals contact the nasals anteromedially, the prefrontals laterally, the postorbitals posterolaterally, and the preparietal posteromedially (Figs. 3A; 4A). The naso-frontal suture is relatively straight in *Repelinosaurus* (Figs. 3A; 4A), whereas it has a distinct posterior process in *Counillonia* (Fig. 2A). No postfrontals are observed in LPB 1995-9 (Fig. 4A) but as in *Counillonia*, we cannot determine whether they were absent or present in LPB 1993-2 because of the eroded external bone surface (Figs. 2A; 3A).

In LPB 1993-2, the preparietal is depressed and bordered anteriorly by a ridge (Fig. 3A), which continues into the median frontal ridge. The surface of the preparietal is flush with the depressed surface of the frontals in LPB 1995-9 (Fig. 4A). The preparietal contacts the postorbitals posterolaterally, the short parietals posteriorly, and the frontals anteriorly (Figs. 3A; 4A).

The parietal contribution of the skull roof in LPB 1993-2 is limited to a midline groove between the posterior postorbital processes (Fig. 3A). These posterior parietal processes are thus slender. Noticeable lateral compression has modified the angulation of the postorbitals in LPB 1995-9. This taphonomic deformation may have resulted in artificial contact of the postorbitals in the midline of the intertemporal bar (Fig. 4A). The posterior expansion of the parietals is dorsally hidden by the posterior processes of the postorbitals or cannot be determined due to the lack of a clear suture between the parietal and interparietal. However, the anterior part of the parietals is preserved. In both specimens of *Repelinosaurus*, the anterolateral processes of the parietals, bordering the pineal foramen, are more anteroposteriorly elongate than broad (Figs. 3A; 4A), but their posterior end is not visible. The external dorsal surface of the parietals contacts the interparietal posteriorly, the postorbitals posterolaterally, and the preparietal anteriorly. The parietals surround the pineal foramen posteriorly with the preparietal anteriorly. The oval pineal foramen is clearly smaller in LPB 1993-2 (0.96 cm of length and 0.66 cm of width) than in LPB 1995-9 (1.33 cm of length and 0.87 cm of width) (Table 2). In both specimens, the foramen is perpendicular to the intertemporal bar and flush with the skull roof. The pineal foramen is also more anterior in LPB 1995-9 than in LPB 1993-2 (continuous character 6, Appendix 1). In ventral view, the preservation of the specimens of

Repelinosaurus does not allow observation of the sutural contact between the parietals and the prootic (Figs. 3B; 4B).

The lateral postorbital bars possess tuberosities in LPB 1993-2, in contrast to LPB 1995-9 (Figs. 3A, B; 4A, B). The posterior postorbital processes of *Repelinosaurus* extend over the entire narrow intertemporal bar as in *Counillonia* (Figs. 2D; 3B; 4B). The temporal portion of the postorbitals is flat and dorsally directed in LPB 1993-2 (Fig. 3A). We consider that its slightly oblique direction in LPB 1995-9 is due to lateral compression (Fig. 4A). This horizontal expansion of the posterior processes of the postorbitals in *Repelinosaurus* is linked to a large fossa formed by the postorbitals and the parietals below the intertemporal bar. The posterior processes of the postorbitals, widened in both LPB 1993-2 and LPB 1995-9, contact the squamosals and the interparietal posteriorly. Anteriorly, they are separated from the preparietal and the parietals by a sharp ridge in LPB 1995-9 (Fig. 4A). The postorbital surface has a triangular depression between the posterior and lateral processes (Figs. 3A; 4A). The lateral process of the postorbitals constitutes the posterior margin of the orbits. They are wider in LPB 1993-2 than in LPB 1995-9 (Figs. 3B; 4B). In LPB 1995-9, they have a sutural contact with the jugals anteroventrally and the zygomatic squamosal processes posteroventrally (Fig. 4A). The state of preservation of the zygomatic arches of LPB 1993-2 does not provide information about the location of the scarf joints. In dorsal view, the lateral expansion of the postorbital bars is smaller in *Repelinosaurus* than in *Counillonia*, giving the skull of *Repelinosaurus* a narrower appearance (Figs. 2A; 3A; 4A).

The lateral surface of the maxilla displays stronger rugosities in LPB 1993-2 than in LPB 1995-9 (Figs. 3B; 4B), but it is difficult to determine the degree to which these rugosities are a real feature. In both skulls, the maxillae contact the premaxilla

anteriorly, and the lacrimals and nasals dorsally. However, in LPB 1993-2, the maxillae do not contact the prefrontals because the anterior process of the lacrimals intervenes, in contrast to LPB 1995-9 (Figs. 3B; 4B; 5). In LPB 1993-2, a notch on the palatal rim is visible on the right side of the skull but not on its left, suggesting a taphonomic origin. The poor preservation of the lateral surface of LPB 1993-2 does not provide information about the sutures in the zygomatic arch. Nevertheless, these contacts are visible in LPB 1995-9 (Fig. 4B). The zygomatic processes of the maxillae comprise a bifid tip embedded in the squamosals and dorsally bordered by the jugals. The maxillae are relatively robust, especially in LPB 1993-2. In addition, the caniniform process is more developed in LPB 1993-2 than in 1995-9 (Figs. 3B; 4B). In *Repelinosaurus* (Figs. 3B; 4B), the caniniform process is vertical, whereas it is anteriorly directed in *Counillonia* (Fig. 2B). The external part of the tusks is missing in LPB 1993-2 but the tusk roots are anteroposteriorly flattened, while they are mediolaterally compressed in LPB 1995-9 (Table 2). In LPB 1995-9, the tusks are posteriorly directed and turn medially, forming a medial concavity (Fig. 4B). The lack of fractures and the direction of the main taphonomic distortion (see above) suggest that the tusks have not been deformed, but the space left between the tusks would not be sufficient to insert a jaw (J. Camp, pers. comm., 2017). Moreover, the distinct wear facet (formed as the mandible slides, e.g., Cluver, 1971; K. Angielczyk, pers. comm., 2018) observed on the inner surface of the left tusk, is backwardly directed, indicating distortion. The distal part of the right tusk is too eroded to reach any conclusion. On the ventral orbital edge, a rounded labial fossa is visible posterior to the caniniform process (Figs. 3C; 4C). Nevertheless, as noted in *Counillonia*, the sutural contacts cannot be discerned; therefore, we cannot conclude whether

Repelinosaurus has a true labial fossa (circumscribed by the maxillae, palatines, and jugals) or just a labial foramen (e.g., Angielczyk and Kurkin, 2003).

In LPB 1995-9, the well-preserved septomaxillae form with the maxillae the posteroventral part of the margin of the nares with nasals dorsally, and the premaxilla anteriorly, where they bear a sharp ridge, which partly divides the nares (Figs. 4B; 5).

The lacrimals are limited by the nasals anteriorly, the prefrontals dorsally, the maxillae anteroventrally, and the jugals posterolaterally in LPB 1993-2 (Fig. 3B). Their anterior well-developed expansion does not allow a sutural contact between the maxillae and the prefrontals. On the lateral surface of LPB 1995-9, the lacrimals are only limited by the maxillae anteriorly and slightly by the jugals posterolaterally (Fig. 4B). A sutural contact between the maxillae and the prefrontals is also reported in some dicynodonts such as *Kombuisia* (e.g., Fröbisch, 2007) or *Kannemeyeria* (e.g., Renaut, 2000). Nevertheless, the antorbital margin formed by the prefrontals, the lacrimals, and the maxillae (Figs. 4B; 5) seems to be unique in LPB 1995-9 within dicynodonts. We cannot therefore rule out the possibility that the limits of the lacrimals may be inaccurate due to taphonomic deformation. Additionally, the left lateral side of the skull is too eroded and this particular bone contact cannot be confirmed. On both skulls of *Repelinosaurus*, the bone sutures of the orbits are not visible (Figs. 3A; 4A). In LPB 1995-9, the lacrimals show a tuberosity on the antorbital rim, which forms the anterior border of the lacrimal foramen.

The jugals make a small contribution to the lateral surface of the skulls (Figs. 3B; 4B). In LPB 1993-2, their sutures with the other bones on the zygomatic arches (except the maxillae and lacrimals) cannot be determined because of poor preservation. The zygomatic arches of LPB 1995-9 show a sutural contact between

the jugals and the postorbitals posteriorly, and the squamosals posteroventrally (Fig. 4B).

The zygomatic squamosal processes form the posterior regions of the zygomatic arches, and circumscribe the temporal fossae laterally and partly posteriorly. They widen posteriorly into a wing-shaped processes and become narrow, without dorsoventral expansion posterior to the postorbital bar (Fig. 3A, B). The right zygomatic arch of LPB 1993-2 presents a ventral expansion at the intersection between the descending bar of the postorbital and the zygomatic arch (Fig. 3B), somewhat reminiscent of the ventrally directed convexity of the squamosal in *Aulacephalodon* (e.g., Tollman et al., 1980). However, the lack of the left zygomatic arch and of visible sutures in the right zygomatic arch does not permit us to conclude whether it is of natural or taphonomic origin. LPB 1995-9 does not exhibit this type of ventral expansion on its zygomatic arches (Fig. 4B). The edge of the zygomatic squamosal wing is flat and straight in LPB 1993-2 (Fig. 3B). The lateral compression affecting LPB 1995-9 has distorted the edge of the zygomatic arch. The squamosal zygomatic processes of LPB 1995-9 contact the jugals and the postorbitals dorsally, and the maxillae in the pointed anterior region (Fig. 4B). In contrast to *Counillonia* (Fig. 2D), the squamosal zygomatic processes of *Repelinosaurus* are inserted dorsally on the back of the skull, well above the dorsal edge of the foramen magnum (Figs. 3D; 4D). They extend slightly onto the dorsal region of the occiput in LPB 1993-2 but not in LPB 1995-9 (Figs. 3B; 4B) because of lateral compression. This compression also raised the intertemporal region and crushed the zygomatic squamosal processes in LPB 1995-9. The temporal squamosal processes of *Repelinosaurus*, delimiting the temporal fossae posteromedially, are shorter than in *Counillonia*. They contact the postorbitals dorsally and the interparietal medially. As

already noted, the bone contact on the occipital side cannot be traced (Figs. 3D; 4D). No conclusion is thus possible concerning the limits of the tabulars and the potential separation of the squamosals and supraoccipitals. The quadrate rami of the squamosals are laterally expanded in *Repelinosaurus*. Compared to *Counillonia* (Fig. 2D), they are in the same plane as the occiput surface in LPB 1993-2 (Fig. 3D). This structure cannot be compared in LPB 1995-9 because of deformation and because of the left quadrate ramus of the squamosal is missing.

The lateral surface of the skulls is eroded but some structures can be made out: a deep anteroventral depression in the squamosal may indicate their contact with the missing quadrate in LPB 1993-2 and in the left side in LPB 1995-9 (Figs. 3B; 4B). In addition, the dorsal head of the epipterygoid contacting the parietals and the basal region of the pila antotica are preserved in LPB 1995-9 (Fig. 4B).

The vomer is missing in LPB 1993-2 but its poorly-preserved anterior region can be observed (Fig. 3C). It displays a median blade separating the choanae in LPB 1995-9 (Fig. 4C). The width of this blade is constant throughout its length. Anteriorly, the vomer shows a tuberosity following the posteromedial ridge of the premaxilla (Figs. 3C; 4C). The vomer is divided posteriorly and delimits the anterior edge of the interpterygoid vacuity, where it contacts the median plate of the pterygoids (Fig. 4C).

The palatines are bordered by the anterior rami of the pterygoids laterally (Figs. 3C; 4C) and the maxillae anteriorly. Because of the poor preservation, the morphology of the palato-premaxillary contact is uncertain. Only the wide anterior region of the palatines is preserved in LPB 1993-2 (Fig. 3C), but their poor preservation does not provide relevant information about their texture. In LPB 1995-9, the palatines widen anteriorly, forming a rugose textured pad (Fig. 4C). No foramen is observed within the palatines, and we cannot determine whether there is

a foramen between these palatines and the anterior rami of the pterygoids because of lateral compression of the palate.

Due to the multiple breaks and the missing bone in some areas, nothing can be said about the presence of pterygoid keels in LPB 1993-2 (Fig. 3B). The ventral projection of the anterior rami of the pterygoids does not strongly extend ventrally in LPB 1995-9 (Fig. 4B), in contrast to *Counillonia* (Fig. 2B) where this extension projects strongly ventrally. However, as in *Counillonia*, the absence of sutures in lateral view prevents measurements of the ventral expansion of the pterygoid keel from being taken. The thin anterior rami of the pterygoids contact the ectopterygoids anterolaterally, in the form of a slender leaf in LPB 1995-9. The ectopterygoids do not expand further posterior to the palatines in palatal view. In LPB 1993-2, they are not preserved but a shallow depression on the anterolateral edge of the pterygoids marks their presence. In LPB 1995-9, the teardrop-shaped interpterygoid vacuity is bordered by the median plate of the pterygoids posteriorly and the vomer anteriorly (Fig. 4C). The anterior margin of the interpterygoid vacuity is not defined in LPB 1993-2 because the major portion of the vomer is missing. As in *Counillonia,* the ventral surface of the median plate bears a thin crista oesophagea in LPB 1995-9, which turns into two ridges posteriorly on the parabasisphenoid (Fig. 4C). However, the bone surface of LPB 1993-2 is eroded. The preservation of the two skulls of *Repelinosaurus* excludes any comments about a potential contribution of the parabasisphenoid to the interpterygoid vacuity. The posterior rami of the pterygoids are poorly preserved in LPB 1993-2 and are missing in LPB 1995-9 (Figs. 3C; 4C).

Two ridges extend onto the parabasisphenoid, from the crista oesophagea, and widen posteriorly (Figs. 3C; 4C). They delimit a broad triangular intertuberal depression. The parabasisphenoid is mainly vertical and makes less contribution to

the fenestra ovalis than the basioccipital. The stapedial facet in LPB 1993-2 is exposed ventrolaterally and its narrow margin extends anteroposteriorly (Fig. 3C). In LPB 1995-9, the structure of the parabasisphenoid-basioccipital tubera is distorted, probably because of taphonomic deformation. As in *Counillonia*, the paired carotid canals, located in the anterior region of the parabasisphenoid, are not visible in either of the specimens of *Repelinosaurus*. No intertuberal ridge is visible. In LPB 1993-2, the basioccipital extends onto the occipital plate and with the exoccipital forms a tripartite occipital condyle (Fig. 3D). The occipital condyle is too poorly preserved in LPB 1995-9 to be precisely described (Fig. 4D).

Only the right quadrate is preserved in LPB 1995-9 (Fig. 4C, D). It is ventrally bifid, with lateral and medial condyles separated by a median groove. The lateral condyle is more anteroposteriorly elongated than the medial one. However, the dorsal lobe was laterally crushed.

The contact between the interparietal and the other bones forming the occiput and the posterior region of the skull roof cannot be discerned (Figs. 3D; 4D). However, it seems that the interparietal does not contribute to the skull roof. In both LPB 1993-2 and LPB 1995-9, the interparietal seems to form a deep longitudinal notch, which is mainly overhung by the postorbitals dorsally. However, the interparieto-parietal suture is not clearly visible.

The occiput is rectangular in LPB 1993-2 (Fig. 3D) but distorted in LPB 1995-9 (Fig. 4D). The insertion of the squamosals on the occiput makes an obtuse angle in LPB 1993-2 (Fig. 3D): most of the lateral squamosal expansion is thus visible in occipital view, in contrast to *Counillonia* (Fig. 2D). The lateral compression of LPB 1995-9 may explain the sharper angle of the lateral squamosal expansions and their asymmetry. As mentioned above, sutures are not clearly preserved. Nevertheless, as

in *Counillonia*, the overall similarity of the occiputs of *Repelinosaurus* (Figs. 3D; 4D) to *Lystrosaurus* (Cluver, 1971), *Dicynodon* or *Diictodon* (Cluver & Hotton III, 1981) suggests that they shared a similar construction of the occiput. However, the dorsoventral expansion of the tabular cannot be determined. In LPB 1995-9, a short nuchal crest, which is ventrally bordered by a depression, extends onto the most dorsal region of the supraoccipital (Fig. 4D). No nuchal crest is visible in LPB 1993-2. A very wide triangular depression extends laterally to the foramen magnum and surrounds the postemporal fenestrae (Figs. 3D; 4D). The anterior tip of this depression is located near the junction between the root of the squamosal wings and the supraoccipital. Its ventral base extends between the basal tubera and the oblique opisthotic crest, which turns into a sharp process.

PHYLOGENETIC ANALYSIS

Methodology

A phylogenetic analysis is used to test the systematic position of the three Laotian dicynodont specimens. This analysis is based on an augmented version of the matrix of Angielczyk and Kammerer (2017), which is one of the most recent and comprehensive analyses of dicynodonts. Our final data set thus includes 106 operational taxonomic units and 194 characters: 171 discrete characters (treated as of equal weight and as unordered, except for characters 81, 84, 102, 163, 173, and 174 following Angielczyk and Kammerer, 2017), and 23 continuous characters (Supplementary Data 1–2). All new measurements and codings, made for the Laotian specimens studied (Appendix 1), are defined using procedures mentioned in

Kammerer et al. (2011) and personal comments from C. F. Kammerer (2017) and K. D. Angielczyk (2017). The treatment of the continuous characters is additive, following Goloboff et al. (2006). Unknown and/or inapplicable states of discrete and continuous characters are coded as "?" (Strong and Lipscomb, 1999). In order to treat the continuous characters with a continued and ordered evolution permitted by Goloboff's algorithm (Goloboff et al., 2006), we analyzed the data set using TNT 1.1 (December 2013 version) (Goloboff et al., 2008). We performed two analyses: a new technology search that analyzes different parts of the tree separately (Goloboff, 1999) and a traditional search. In the first case, we did a driven search with the initial search level set checked every three hits. One hundred replications were chosen as a starting point for each hit and we required to search to find the most parsimonious trees twenty times. We did the phylogenetic analysis using sectorial search (default settings) and tree-drifting (default settings but the number of cycles was 3) to produce a nearly optimal tree, which could be used for tree-fusing (default settings but a global fuse every 3 hits was input; Goloboff, 1999). In the second search, we used a traditional search of TBR branch swapping with 11,111 replications and 9 trees saved per replications. *Biarmosuchus* was used as an outgroup. We obtained the same most parsimonious tree with both methods (1156.346 steps, CI = 0.236, RI = 0.712) (Fig. 6). We indicate the Bremer values as a node support index (Fig. 6; Bremer, 1988). According to the recommendations of Goloboff et al. (2008), we performed successive traditional searches using the most parsimonious trees as a starting point. We increased the value of suboptimal trees each step to avoid overestimation of the value of the Bremer support. We saved successively larger sets of suboptimal trees ("stop when maxtrees hit" ticked on). The resulting trees were checked to discard duplicate cladograms each search. Once the optimal and suboptimal trees stored

(99,999 unique cladograms), we tested the score differences to lose each node using "Bremer support" function.

Results and Comparisons with Previous Dicynodont Phylogenies

The most parsimonious tree obtained (Fig. 6) is completely resolved. The clade Dicynodontoidea is weakly supported. However, some clades within Dicynodontoidea are well supported, such as Rhachiocephalidae and Lystrosauridae (Fig. 6).

We hereafter follow the comprehensive taxonomy of Kammerer and Angielczyk (2009). Our results are in accordance with the strict consensus cladogram of Angielczyk and Kammerer (2017), except for some relationships within Dicynodontoidea. Our phylogenetic analysis indicates that Pylaecephalidae are distinct from Emydopoidea, not recovered within Therochelonia, and placed in a comparable position to that proposed by Angielczyk and Kurkin (2003), Fröbisch (2007), Angielczyk and Rubidge (2013), Boos et al. (2016), Angielczyk and Kammerer (2017) and Angielczyk et al. (2018). Additionally, the Kingoriidae are here included in the Kistecephalia within Emydopoidea as previously proposed (e.g., Angielczyk and Kurkin, 2003; Angielczyk and Rubidge, 2013; Castanhinha et al., 2013; Cox and Angielczyk, 2015; Angielczyk et al., 2016; Angielczyk and Kammerer, 2017; Kammerer and Smith, 2017; Angielczyk et al., 2018). Within dicynodontoids, the relationships within Cryptodontia (here compositionally equivalent to Oudenodontidae), Rhachiocephalidae, and Lystrosauridae are consistent with the results of Angielczyk and Kammerer (2017). In contrast to previous studies (e.g., Angielczyk and Rubidge, 2013; Castanhinha et al., 2013; Kammerer et al., 2013; Cox and Angielczyk, 2015; Kammerer and Smith, 2017), Rhachiocephalidae and Geikiidae are not included in Cryptodontia, but in Dicynodontoidea (as defined by

Kammerer and Angielczyk, 2009) as proposed by Boos et al. (2016), Angielczyk and Kammerer (2017), and Angielczyk et al. (2018).

As mentioned by Kammerer and Angielczyk (2009), no consensus exists about a taxonomic definition of Kannemeyeriiformes, probably because the alpha taxonomy of the Triassic forms is still unresolved. If we consider the definition of Kannemeyeriiformes sensu Maisch (2001) as the clade of Triassic non-lystrosaurid dicynodontoids, in our current results, the Laotian *Repelinosaurus* may thus be considered as a kannemeyeriiform. However, the other Laotian Triassic genus *Counillonia* is a non-kannemeyeriiform dicynodontoid, closely related to Permian "*Dicynodon*"-grade taxa (i.e., most taxa previously attributed to *Dicynodon* before the taxonomic revision by Kammerer et al., 2011): *Daptocephalus*, *Peramodon*, *Dinanomodon*, *Turfanodon*, *Euptychognathus*, *Sintocephalus*, *Jimusaria*, *Gordonia*, *Delectosaurus*, *Vivaxosaurus,* and the two valid species of *Dicynodon* (Fig. 6; Kammerer et al. 2011). The stratigraphic definition of Kannemeyeriiformes sensu Maisch (2001) is thus challenged by the phylogenetic position of *Counillonia*. We therefore follow the phylogenetic definition of Kannemeyeriiformes sensu Kammerer et al. (2013) as the clade comprising *Kannemeyeria simocephalus* and all taxa more closely related to it than to *Lystrosaurus murrayi* or *Dicynodon lacerticeps*. Under this definition, *Repelinosaurus* is recovered as a kannemeyeriiform. In contrast to recent studies, our phylogeny recovers a large clade of "*Dicynodon*"-grade taxa uniting *Daptocephalus*, *Peramodon*, *Dinanomodon*, *Turfanodon*, *Euptychognathus*, *Sintocephalus*, *Jimusaria*, *Gordonia*, *Delectosaurus*, *Vivaxosaurus,* and the two valid species of *Dicynodon* (Kammerer et al. 2011). These "*Dicynodon*"-grade taxa and *Counillonia* form a clade with Kannemeyeriiformes characterized by two non-ambiguous synapomorphies: (1) a lacrimal not in contact with the septomaxilla

(60(0)) and (2) a dorsal process on the anterior end of the epipterygoid footplate (127(1)). The results of Angielczyk and Kurkin (2003) also recovered *Peramodon* and *Vivaxosaurus* as more closely related to Kannemeyeriiformes than to *Lystrosaurus*. Within Kannemeyeriiformes, our phylogenetic results indicate that *Repelinosaurus* is sister to the rest of kannemeyeriiform, which is divided into three relatively well-supported clades: Shansiodontidae, Kannemeyeriidae, and Stahleckeriidae. Shansiodontidae, as defined by Maisch (2001), includes *Shansiodon*, *Vinceria, Rhinodicynodon*, and *Tetragonias*. They are sister group to all other kannemeyeriiforms but *Repelinosaurus*, a position previously recovered by Castanhinha et al. (2013), Kammerer et al. (2013), Cox and Angielczyk (2015), Boos et al. (2016), and Kammerer and Smith (2017). Despite the fact that Shansiodontidae sensu Maisch (2001) are paraphyletic in the analyses of Kammerer and Angielczyk (2017) and Angielczyk et al. (2018), *Shansiodon*, *Vinceria, Rhinodicynodon*, and *Tetragonias* are also more basal than all other kannemeyeriiforms in their studies. The compositions of the clades Kannemeyeriidae and Stahleckeriidae are similar in the current analysis to those of Kammerer and Angielczyk (2017) and Angielczyk et al. (2018). Stahleckeriidae, as the last common ancestor of *Placerias hesternus* and *Stahleckeria potens,* and all of its descendants, excluding *Shansiodon wangi* or *Kannemeyeria simocephalus* (Kammerer et al., 2013), are characterized by six non-ambiguous synapomorphies: (1) a short interpterygoid vacuity (continuous character 10); (2) a very reduced minimum width of the scapula (continuous character 17); (3) a very long anterior iliac process (continuous character 21); (4) a smooth and flat median pterygoid plate (115(1)); (5) the presence of six sacral vertebrae (165(3)); and (6) the M. latissimus dorsi inserted on a rugose tuberosity on the posteroventral surface of the humerus (175(0)). Kannemeyeriidae may therefore be defined here as

the clade comprising *Kannemeyeria simocephalus* and all taxa more closely related to it than to *Stahleckeria potens*, *Placerias hesternus,* or *Shansiodon wangi*. This clade is supported by six non-ambiguous synapomorphies: (1) a high preorbital region (continuous character 1); (2) a high trochanteric crest on the femur (continuous character 22); (3) a very narrow scapula (the narrowest in dicynodontoids; continuous character 23); (4) a dorsal edge of the erupted portion of the canine tusk anterior to the anterorbital margin (55(0)); (5) a temporal portion of the skull roof angled dorsally with a strong break in slope near its anterior end (67(1)); and (6) a lateral edge of the paroccipital process distinctly offset from the surface of the occipital plate (135(1)).

Positions of the three Laotian specimens

Our results indicate that the Laotian specimens LPB 1993-2 and LPB 1995-9 form a relatively well-supported clade, characterized by five non-ambiguous synapomorphies: (1) the most reduced preorbital region in dicynodontoids (continuous character 1); (2) a notch on the dorsal edge of the narial opening (41(1)); (3) nasal bosses present as a median swelling with a continuous posterior margin (57(1)); (4) parietals exposed in the midline groove (72(1)); and (5) a relatively flat temporal portion of the postorbitals, so that most of the external surface of the bone faces dorsally (74(0)). This supports our attribution of these Laotian specimens to the single new taxon *Repelinosaurus robustus* gen. et sp. nov. erected above. This Laotian clade is included in Kannemeyeriiformes, which are thus defined by three derived character states: (1) the absence of postfrontal (64(1)); (2) no converging ventral keels on the posterior portion of the anterior pterygoid rami (114(0)); and (3) the absence of the intertuberal ridge (126(0)).

As already mentioned, the third Laotian specimen LPB 1993-3 is close to some "*Dicynodon*"-grade taxa: *Daptocephalus*, *Peramodon*, *Dinanomodon*, *Turfanodon*, *Euptychognathus*, *Sintocephalus*, *Jimusaria*, *Gordonia*, *Delectosaurus*, *Vivaxosaurus,* and the two valid species of *Dicynodon* (Kammerer et al. 2011). All these taxa form a clade supported by four non-ambiguous synapomorphies: (1) the highest temporal fenestra within dicynodontoids (continuous character 5); (2) a weakly-developed distal end of the radius in contrast to the other dicynodontoids (continuous character 19); (3) a rounded anterior tip of the snout (35(0)); and (4) a raised circumorbital rim (62(1)). Within this clade, LPB 1993-3 is sister to the clade formed by the late Permian South Gondwanan *Daptocephalus* and *Dinanomodon*, Chinese *Turfanodon,* and Russian *Peramodon* (Fröbisch, 2009).

Battail (2009) previously compared the three Laotian specimens with *Lystrosaurus* and *Dicynodon*. Based on a morphological study, he attributed them to *Dicynodon* as previously defined by Cluver & Hotton III (1981), before the taxonomic revision of *Dicynodon* by Kammerer et al. (2011). Our phylogenetic results do not contradict this preliminary assignment because the Laotian specimens show closer affinities with "*Dicynodon*"-grade taxa and the two valid species of *Dicynodon* (Kammerer et al. 2011) than with *Lystrosaurus*.

DISCUSSION

Morphological Variation in *Repelinosaurus robustus*

LPB 1995-9 and LPB 1993-2 are found in the same clade as *Repelinosaurus*, which is an early kannemeyeriiform (Fig. 6). As noted above, a variety of features

distinguishes these two specimens. However, these differences could be related to postmortem distortions, ontogeny, sexual dimorphism or other intraspecific variation.

LPB 1995-9 is distinguished by well-defined depressions lateral to the median ridge of the premaxilla in contrast to the flat surface in LPB 1993-2 (discrete character 29, Appendix 1). Nevertheless, it is clear that LPB 1995-9 was affected by lateral compression, as indicated by the lack of symmetry in ventral view, the tusks turned inward, the more anterior position of the left tusk with respect to the right one, and breaks in the compressed zygomatic arches. In addition, the angulation between the occipital plate and the palate is less in LPB 1995-9 than in LPB 1993-2 (continuous character 13, Appendix 1) and could be linked to taphonomic distortion. This latter could also explain other differences such as (1) the direction of the posterior processes of the postorbitals (slightly oblique in LPB 1995-9 but horizontal in LPB 1993-2); (2) the insertion of the squamosal wings in the occipital plate (reaching the dorsal margin of the occiput in LPB 1993-2 but not in LPB 1995-9); and (3) the dorsal expansion of the parietals in the intertemporal bar (as a midline groove in LPB 1993-2 but mostly overlapped by the postorbitals in LPB 1995-9). In addition, although only two specimens of *Repelinosaurus* are currently known, it cannot excluded that the other morphological differences between the two specimens could be related to ontogenetic, dimorphic or other intraspecific variation.

Indeed, the negative allometry measured in the length of the pineal foramen versus skull size in *Repelinosaurus* (Table 2) could be interpreted as ontogenetic variability, as observed in *Colobodectes cluveri* (Angielczyk and Rubidge, 2009). In this taxon, Angielczyk and Rubidge (2009) also noted well-developed caniniform processes with a disappearance of the palatal rim notch in the largest skull. Here, the large LPB 1993-2 shows a deeper lateral convexity of the caniniform processes, yet

no palatal rim notch is present. A greater length of the intertemporal bar posterior to the pineal foramen is also noted in the smaller LPB 1995-9 (continuous character 6, Appendix 1), as is the case in the Middle Triassic *Dolichuranus primaevus* (C. Olivier, pers. obs., 2018, on BP/1/4570 vs. BP/1/4573). This could suggest that the position of the pineal foramen may be related to ontogeny.

LPB 1995-9 is less robust than LPB 1993-2, which bears more developed ornamentations: (1) its frontals bear a sharp frontal ridge; (2) high rugosities are noted on its premaxilla, maxillae, lateral processes of the postorbitals, and the squamosal zygomatic arch; and (3) its nasal bosses are more laterally developed. Variations in width, depth, and rugosity of skulls of the Middle–Late Triassic *Dinodontosaurus turpior* appear to be related to ontogeny (e.g., C. Olivier, pers. obs., 2018; Lucas and Harris, 1996): the large specimen MCZ 1679 bears frontal, prefrontal, and postorbital bosses, which contrast with the smaller MCZ 1677 (C. Olivier, pers. obs., 2018). The development of cranial ridges and ornamentations are indeed related to skull size in *Lystrosaurus*, but only up to a size threshold (Grine et al., 2006). In addition, the size variation of ridges and ornamentations differs according to the species of *Lystrosaurus* (Grine et al., 2006). More developed ornamentations are also observed in the largest skulls of *Lystrosaurus*, but Ray (2005) supposed a sexually dimorphic variation, with inferred male individuals more ornamented than females. In addition, a more developed cranial ornamentation in adult males has been evidenced in *Diictodon* (Sullivan et al., 2003) and in *Pelanomodon*, which may be linked to the ‘armament’ in the context of sexual selection (Kammerer et al., 2016). The relative form and size of the nasal bosses also appears to be related to sexual dimorphism in the Permian *Aulacephalodon* (e.g., Keyser, 1969; Tollman et al., 1980). However, the quantitative analyses of

Tollman et al. (1980) indicated a positive allometry in the width of the nasal bosses, instead suggesting an ontogenetic effect on it in *Aulacephalodon*. Moreover, as seen in LPB 1993-2, a ventrally directed convexity of the squamosal zygomatic arch in large specimens of *Aulacephalodon* are observed only in males (e.g., Tollman et al., 1980).

The basal section of the tusk of LPB 1993-2 (anteroposteriorly compressed) is different from that of LPB 1995-9 (mediolateraly compressed) (Table 2). Angielczyk and Rubidge (2009) noted the fact that the smallest specimen of *Colobodectes cluveri* has less-developed and newly erupted tusks, is related to ontogeny. In *Repelinosaurus*, the tusks of LPB 1995-9 are well erupted and in the same proportion as in the larger LPB 1993-2. This variation in the basal section of the tusk thus appears unlikely to be linked to ontogeny. The mediolateral compression of the tusks in LPB 1995-9 could not be explained by lateral postmortem compression because of the excellent preservation of the tusks. Another intraspecific variation (i.e. related neither to sex nor to ontogeny) may thus explain the differences in tusk basal sections. This may also be the case for the preparietal depressed or flush with the skull roof (discrete character 68, Appendix 1) and for the maxillo-prefrontal suture, which is either present only in some of the specimen (discrete character 49, Appendix 1).

Most morphological variation within *Repelinosaurus robustus* may therefore be related to ontogeny and/or sexual dimorphism demonstrated to occur in other dicynodonts (e.g., Keyser, 1969; Tollman et al., 1980; Ray, 2005; Angielczyk and Rubidge, 2009), taphonomic distortion or other intraspecific variation. Nevertheless, as mentioned above, the number of specimens of *Repelinosaurus* is too low to

assess which kind of intraspecific variation (sexual dimorphism, ontogeny, etc.) is present.

Taxonomic validity of *Repelinosaurus* and *Counillonia*

Phylogenetic affinities are found between the Laotian *Counillonia* and the late Permian *Peramodon*, *Delectosaurus*, *Vivaxosaurus, Turfanodon*, *Jimusaria*, *Gordonia*, *Euptychognathus*, *Daptocephalus*, *Dinanomodon*, *Sintocephalus,* and the two valid species of *Dicynodon* (Fig. 6; Kammerer et al. 2011). Within the clade formed by *Counillonia* and these "*Dicynodon*"-grade taxa, the following autapomorphies distinguish the Laotian dicynodont: (1) a relatively large median pterygoid plate (continuous character 8, Appendix 1), (2) the absence of an intertuberal ridge; and (3) opisthotics with distinct posteriorly-directed processes (Figs. 2C–D). As in *Delectosaurus*, the occipital condyle of *Counillonia* is not fused, while the other cited "*Dicynodon*"-grade taxa have a co-ossified single unit. The naso-frontal suture is either straight, as in *Dicynodon huenei* and *Jimusaria*, or has an anterior process in the other cited "*Dicynodon*"-grade taxa, unlike the clear posterior process in *Counillonia* (Fig. 2A). Overall, most morphological characters distinguish *Counillonia* from its closely related "*Dicynodon*"-grade taxa. If we focus on the geographically close taxa such as the Russian *Peramodon*, *Delectosaurus* and *Vivaxosaurus,* and the Chinese *Turfanodon* and *Jimusaria*, other differences can be highlighted. *Peramodon* and *Turfanodon* have a rounded dorsal margin of the squamosal wings in lateral view (Kammerer et al., 2011), while it is more acute in *Counillonia* because of a lower lateral opening (Fig. 2B). The interorbital region in *Turfanodon* is wider than in *Counillonia* (Fig. 2A; Kammerer et al., 2011). *Counillonia* also has an interpterygoid vacuity and temporal squamosal processes longer than in

Jimusaria (Kammerer et al. 2011); the squamosals therefore do not reach the dorsal region of the occiput in this Laotian genus (Fig. 2B). In contrast to *Vivaxosaurus*, the caniniform processes are less anteriorly projected in *Counillonia*, and its maxillae do not bear a rounded boss anterior to the tusks (Fig. 2B; Kammerer et al., 2011). In *Counillonia*, the anterior rami of the pterygoids are ventrally highly expanded and therefore not in the same plane as the more dorsal palatines (Fig. 2C), in contrast to *Delectosaurus*.

Repelinosaurus is recovered as a kannemeyeriiform. Only one genus of kannemeyeriiform was previously known near the Permo–Triassic boundary: the Early Triassic *Sungeodon* (Maisch & Matzke, 2014). *Repelinosaurus* differs from all kannemeyeriiforms by the strong reduction of the preorbital region (Figs. 3A; 4A). This character state is shared to a lesser degree with *Counillonia* (Fig. 2A) and the kistecephalian *Kombuisia* (Fröbisch, 2007). As in the Early Triassic *Kombuisia* and *Myosaurus*, the nasal bosses of *Repelinosaurus* form a single median swelling in dorsal view (Figs. 3A; 4A), in contrast to currently known kannemeyeriiforms that have a pair of bosses. In *Repelinosaurus*, the parietals, weakly exposed on the skull roof, are inserted between the two wide posterior processes of the postorbitals (Figs. 3A; 4A), in contrast with the majority of kannemeyeriiforms except *Sangusaurus*, *Uralokannemeyeria,* and *Rechnisaurus*. Kannemeyeriiformes are known for their temporal crest, generally associated with laterally-directed posterior processes of the postorbitals. This is not the case in *Repelinosaurus* (Figs. 3A–B; 4A–B), where the postorbitals mainly face dorsally.

New Data Supporting the Survivorship of Multiple Lineages across the P–Tr Boundary?

The latest Permian terrestrial biomes were dominated by herbivorous pareiasaurs and dicynodonts, and carnivorous gorgonopsians and therocephalians (e.g., Steyer, 2012; Benton and Newell, 2014). A recent study (Bernardi et al., 2017) evidenced a link between the distribution of herbivore tetrapods, phytoprovinces and latitudinal climatic zonation. More specifically, dicynodonts were predominant only in high paleolatitudes biomes. The dicynodonts were strongly affected by the P–Tr crisis (e.g., Fröbisch, 2007). The lystrosaurids are the emblematic clade to have survived the P–Tr event (e.g., Fröbisch, 2007; Botha-Brink et al., 2016). However, as indicated by the dicynodont phylogenetic relationships recovered herein (e.g., Angielczyk, 2001; Fröbisch, 2007, 2010; Kammerer et al., 2011), other lineages also appear to cross the end-Permian boundary. Fröbisch (2007) previously highlighted the interesting phylogenetic position of the Triassic *Kombuisia*, belonging to kingoriids and closely related to the Permian *Dicynodontoides*. *Kombuisia* is known from the probable Middle Triassic of South Africa and also the Early Triassic of Antarctica (e.g., Fig. 6; Fröbisch, 2007, 2010). The stratigraphic positions of the two *Kombuisia* species imply lengthy ghost lineages, stretching back into the Permian. The Early Triassic *Myosaurus* is also closely related to Permian dicynodonts and is sister taxon to the cistecephalids (e.g., Fig. 6; Fröbisch, 2007). In addition, most previous studies assumed a ghost lineage for Kannemeyeriiformes (e.g., Fröbisch, 2007, 2010; Kammerer et al., 2011). Kammerer et al. (2011) indeed inferred Permian forms (such as lystrosaurids or "*Dicynodon*"-grade taxa) as sister groups to the kannemeyeriiforms. They thus assumed a ghost lineage for the kannemeyeriiforms that spans at least part of the late Permian and the earliest Triassic.

Most previous studies noted the impact of a potential geographic bias on the presence of ghost lineages in dicynodonts (e.g., Angielczyk, 2001; Fröbisch et al.,

2010; Kammerer et al., 2011). Their hypothesis was supported by the discovery of specimens of *Kombuisia* (formerly known from the Karoo Basin in South Africa, dated to the Middle Triassic) from the Early Triassic Fremouw Fm in Antarctica (Fröbisch, 2010). In addition, the assumption of Kammerer et al. (2013) that supposed the occurrence of kannemeyeriiforms in the Early Triassic gained support by the recent description of *Sungeodon* from the Junggar Basin in China (Maisch & Matzke, 2014). Despite relatively weak node supports, the phylogenetic position of the Laotian *Repelinosaurus* also helps to shorten the ghost lineage between the kannemeyeriiforms and the other dicynodontoids, extending the first appearance of Kannemeyeriiformes to near the P–Tr boundary. In addition, the discovery of the earliest kannemeyeriiforms in an understudied geographic area such Laos, with *Repelinosaurus* and China, with *Sungeodon* (Maisch & Matzke, 2014), strengthens these suggestions, underlining a geographic bias in dicynodont sampling. The phylogenetic position of *Counillonia* makes it the first known "*Dicynodon*"-grade dicynodontoid that could have survived the P–Tr extinction (maximum depositional age of 251.0 ± 1.4 Ma).This supports the survivorship of multiple dicynodont lineages across the P–Tr event, as previously suggested (e.g., Angielczyk, 2001; Fröbisch, 2007, 2010; Kammerer et al., 2011).

The dicynodont post-extinction recovery was thought to be have been relatively delayed (e.g., Sahney and Benton, 2008; Chen and Benton, 2012), starting in the Middle Triassic when the kannemeyeriiforms underwent a large adaptive radiation (Fröbisch, 2009). Sun et al. (2012) described an "equatorial tetrapod gap" and attributed the delayed recovery to excessive paleotemperatures during the Early Triassic, especially at the warmer equatorial paleolatitudes. However, other studies have supported a rapid recovery (e.g., Botha and Smith, 2006; Maisch and Matzke,

2014). The occurrence in the Early Triassic of the kannemeyeriiform *Sungeodon* (Maisch and Matzke, 2014) and potentially of a new Laotian kannemeyeriiform *Repelinosaurus* (maximum depositional age of 251.0 ± 1.4 Ma; Rossignol et al., 2016) would support a rapid recovery of the group after the P–Tr mass extinction event. In addition, Bernardi et al. (2018) explained the "equatorial tetrapod gap" defined by Sun et al. (2012) by invoking a northwards tetrapod distribution shift during the Induan. Besides, as for Antarctica (Fröbisch et al., 2010), the presence of dicynodonts (*Repelinosaurus* and *Counillonia*) and a chroniosuchian (*Laosuchus naga*, Arbez et al., 2018) in Laos near the Permo–Triassic boundary may also indicate a refuge zone where the dicynodont and chroniosuchian (and possibly other tetrapod faunas) were not strongly affected by the P–Tr crisis. However, the available data on the Laotian fauna of the Permo–Triassic period is not yet sufficient to draw firm conclusions on this point.

As mentioned above, Bernardi et al. (2017) demonstrated a significant correlation between the distribution of the dicynodonts and phytoprovinces, indicating that the resilience and survivorship of dicynodonts after the crisis may be linked to plant diversity. Indeed, Gastaldo et al. (2017) described an uninterrupted plant cover of glossopterids and sphenophytes in the *Lystrosaurus* Assemblage zone, across the P–Tr boundary. A full recovery of plants is also attested from the Middle Triassic (e.g., Benton and Newell, 2014). An Early Triassic flora is well documented in South China, combining the late Permian relic *Gigantopteris* and pioneer taxa dominated by the lycopsid *Annalepsis* (Yu et al., 2015). This Chinese paleoflora has been shown to be stable across the P–Tr boundary, with the highest turnover rates occurring during the Induan (Xiong and Wang, 2011). Even if documented in a distinct and somewhat remote area from the Luang Prabang Basin at that time (Fig. 1), a rich and diversified

paleoflora (Bercovici et al., 2012) has been evidenced above the strata correlated to the late Changhsingian (Blanchard et al., 2013) and below the Purple Claystone Fm (Rossignol et al., 2016). The occurrence of paleosols with root traces (Bercovici et al., 2012) attests to the presence of plants during the deposition of the Purple Claystone Fm.

Paleobiogeographical Implications of the Two Laotian Dicynodonts

The occurrence of new dicynodonts in the Luang Prabang Basin (Laos), located in the Indochina Block (e.g., Fig. 1A; Cocks and Torsvik, 2013), provides interesting new insights on the controversed paleogeography of Southeast Asia.

Like all the other East and Southeast Asian continental blocks, the Indochina Block originates from the Eastern Gondwana margin (e.g., Metcalfe, 2013; Burrett et al., 2014). The separation of this block from the Gondwana mainland, by the opening of the Paleotethyan Ocean, is dated from the Early Ordovician (e.g., Cocks and Torsvik, 2013) or the Devonian (e.g., Metcalfe, 2011, 2013; Thanh et al., 2011; Lai et al., 2014). The collision between the Indochina and South China blocks has been variously dated: Silurian to Devonian (e.g., Thanh et al., 2011), Carboniferous (e.g., Metcalfe, 2011; Vượng et al., 2013; Zhang et al., 2014), late Permian to Early Triassic (Halpin et al., 2016), Early Triassic (e.g., Lepvrier et al., 2004; Kamvong et al., 2014), Middle Triassic (e.g., Nakano et al., 2008; Zhang et al., 2013, 2014; Faure et al., 2014; Rossignol et al., 2018) or even Late Triassic (e.g., Liu et al., 2012).

Microanatomical studies, analyzing the distribution of the bone tissues, morphological and taphonomic evidence, support an essentially terrestrial lifestyle for most of dicynodonts (e.g., Ray et al., 2005, 2010; 2012; Wall 1983; King and Cluver, 1990; Botha-Brink and Angielczyk, 2010). *Lystrosaurus* is one of the rare dicynodonts

supposed to be semi-aquatic based on its microanatomy, morphology, and taphonomic preservation (e.g., Germain and Laurin, 2005; Ray, 2006). However, these conclusions have been questioned, and a terrestrial lifestyle has been proposed for *Lystrosaurus* based on its microanatomy, associated faunas, and paleoenvironment (e.g., King and Cluver, 1990; Botha-Brink and Angielczyk, 2010). The bone microstructure in *Lystrosaurus* is similar to that of *Placerias*, *Wadiasaurus,* and *Kannemeyeria* (Ray *et al.*, 2005, 2012; Wall 1983). However, whilst a semi-aquatic lifestyle based on microanatomy is proposed for *Placerias* (Green *et al*., 2010), *Kannemeyeria*, and *Wadiasaurus* were supposed to be terrestrial (Ray *et al.*, 2010, 2012). Evidence for dicynodont lifestyle remains equivocal, but even if some taxa did have a semi-aquatic but freshwater lifestyle, this would be unlikely to allow dispersal across a wide oceanic domain.

The presence of dicynodonts in Laos highlights a connection between the Indochina Block and South China Block (SCB). U–Pb geochronology on detrital zircon suggested that the connection may occur not later than 251.0 ± 1.4 Ma, the maximum depositional age. Two different hypotheses can be proposed to account for such a connection.

Firstly, the Indochina Block could have been connected with the North China Block (NCB), via the SCB. This hypothesis requires that the contact between the NCB and the SCB was effective at 251.0 ± 1.4 Ma, i.e, slightly before the Middle to Late Triassic age generally considered plausible for the collision between these blocks (Li, 1994; Weislogel et al., 2006; Chang and Zhao, 2012; Torsvik and Cocks, 2017). It also implies a connection between the Indochina Block and the SCB before or during the latest Permian or earliest Triassic, as proposed by Lepvrier et al. (2004), Metcalfe (2011), Kamvong et al. (2014), Scotese (2014), and Halpin et al.

(2016). However, other interpretations support a continental connection between the SCB and the Indochina Block later than the Early Triassic (see references above). A diachronous continental collision between the SCB and the Indochina Block (Halpin et al., 2016), beginning during the late Permian to the East (present day coordinates) and continuing toward the West up to the Middle Triassic, has recently been put forward. Such a hypothesis reconciles an Early to Middle Triassic collision between the SCB and the Indochina Block with the paleobiogeographic distribution of dicynodonts. This is further corroborated with the discovery of a new chroniosuchian in non-marine rocks in the Purple Claystone Fm (Arbez et al., 2018), which is inferred to have had an amphibious lifestyle (e.g., Buchwitz et al, 2012; Golubev, 2015; Arbez et al., 2018) and which supports a connection between Eurasia and the Indochina Block at that time.

Secondly, another hypothesis to account for the presence of dicynodont remains in the Indochina Block consists of an indirect connection with other landmasses via a string of microcontinents. Indeed, a connection between Pangea and the Indochina Block, involving the western Cimmerian continental strip before or during the Early Triassic, was also suggested (Buffetaut, 1989; Metcalfe, 2006, 2011). Laos is characterized by a Cathaysian flora, also found in China, Korea, Japan, Thailand, Indonesia, and Malaysia (e.g., Bernardi et al., 2017). The high affinities between Cathaysian and Cimmerian faunas and floras suggest geographical proximity (Wang and Sugiyama, 2002; Torsvik and Cocks, 2017). Nevertheless, this proximity is based on plants and marine faunas (Wang and Sugiyama, 2002; Ueno, 2003; Shen et al., 2013; Torsvik and Cocks, 2017), which are less constrained for dispersion by oceanic barriers than terrestrial faunas are. Moreover, the presence of marine faunas and a majority of limestone deposits during the late Permian in the Sibumasu Block

(e.g., Ueno, 2003; Chaodumrong et al., 2007; Shen et al., 2013; Wang et al., 2013), indicate a largely submerged land (Metcalfe, 2011). Furthermore, the collision between the Sibumasu or Simao blocks with the Indochina Block is considered to have occurred after the Norian (e.g., Metcalfe, 2011; Rossignol et al., 2016). The Cimmerian option also supposes proximity between the Cimmerian blocks and Pangea. The collision between Iran and Eurasia is latest Triassic–Jurassic in age (e.g., Wilmsen et al., 2009; Zanchi et al., 2009). However, Zanchi et al. (2015) suggest an affinity and probable proximity between Eurasia and Central Iran as early as late Paleozoic. These uncertainties render difficult the involvement of the Cimmerian blocks during the Permian–Triassic in the role of an indirect connection, and suggest the existence of other microcontinents to explain this second hypothesis.

The aforementioned two hypotheses are based on a maximum depositional age of 251.0 ± 1.4 Ma for the Laotian dicynodonts. Such a maximum depositional age is also compatible with a deposition of the Purple Claystone Fm in the Middle Triassic (Rossignol et al., 2016). This maximum depositional age is therefore consistent with paleogeographic results indicating collisions between NCB and SCB (Li, 1994; Weislogel et al., 2006; Chang and Zhao, 2012; Torsvik and Cocks, 2017) in the Middle Triassic, and between the Indochina Block and SCB in the Middle to Late Triassic (e.g., Liu et al., 2012; Zhang et al., 2013; Faure et al., 2014; Rossignol et al., 2018). This implies the survival of a "*Dicynodon*"-grade taxon *Counillonia superoculis* to the P–Tr crisis. This work brings new insights to ongoing debates about the paleobiogeographic and geodynamic evolution of Southeast Asia from the late Paleozoic to the early Mesozoic. It warrants further field expeditions in late Permian

and Early Triassic formations in the former indochina block to confirm or reject our hypotheses.

ACKNOWLEDGMENTS

We thank the Minister of Information and Culture of Lao PDR and the Savannakhet Dinosaur Museum (Laos) for their authorization to study the material. We also thank C. Bouillet and P. Richir (CR2P, MNHN, Paris, France) for their help during the preparation of the material, S. Fernandez (MNHN) for the drawings, T. Arbez (CR2P, MNHN) for his comments on the Laotian chroniosuchian, B. Khalloufi (CR2P, MNHN) and R. Zaragüeta (ISYEB, MNHN) for their discussion on paleobiogeographic issues, and R. R. Allain, V. Barriel, O. Bethoux, G. Billet, M. Laurin (CR2P, MNHN), A. K. Huttenlocker (University of Southern California, Los Angeles, California, U.S.A.), C. Kammerer (North Carolina Museum of Natural Sciences, Raleigh, North Carolina, U.S.A.), K. D. Angielczyk (Field Museum of Natural History, Chicago, Illinois, U.S.A.), J. Camp (University of California, Riverside, County California, U.S.A.), and an anonymous reviewer for their relevant and constructive remarks, and M. Pickford (CR2P, MNHN) and M. Laurin (CR2P, MNHN) for improving the English. C.O. benefited from the financial support of the GDRI PalBioDiv SEA project, which allowed her to consult the dicynodonts material in Savanaketh (Laos). C.R. acknowledges the financial support of the São Paulo Research Foundation (FAPESP - Fundação Amparo à Pesquisa do Estado de São Paulo; processo 2018/02645-2 and processo 2015/16235-2).

LITERATURE CITED

Angielczyk, K. D. 2001. Preliminary phylogenetic analysis and stratigraphic congruence of the dicynodont anomodonts (Synapsida: Therapsida). Palaeontologica Africana 37:53–79.

Angielczyk, K. D., and C. F. Kammerer. 2017. The cranial morphology, phylogenetic position and biogeography of the upper Permian dicynodont *Compsodon helmoedi* van Hoepen (Therapsida, Anomodontia). Papers in Palaeontology 3:513–545.

Angielczyk, K. D., and A. A. Kurkin. 2003. Phylogenetic analysis of Russian Permian dicynodonts (Therapsida: Anomodontia): implications for Permian biostratigraphy and Pangaean biogeography. Zoological Journal of the Linnean Society 139:157–212.

Angielczyk, K. D., and B. S. Rubidge. 2009. The Permian dicynodont *Colobodectes cluveri* (Therapsida, Anomodontia), with notes on its ontogeny and stratigraphic range in the Karoo Basin, South Africa. Journal of Vertebrate Paleontology 29:1162–1173.

Angielczyk, K. D., and B. S. Rubidge. 2013. Skeletal morphology, phylogenetic relationships and stratigraphic range of *Eosimops newtoni* Broom, 1921, a pylaecephalid dicynodont (Therapsida, Anomodontia) from the Middle Permian of South Africa. Journal of Systematic Palaeontology 11:191–231.

Angielczyk, K. D., B. S. Rubidge, M. O. Day, and F. Lin. 2016. A Reevaluation of *Brachyprosopus broomi* and *Chelydontops altidentalis*, Dicynodonts (Therapsida, Anomodontia) from the Middle Permian *Tapinocephalus* Assemblage Zone of the Karoo Basin, South Africa. Journal of Vertebrate Paleontology 36:e1078342.

Angielczyk, K. D., P. J. Hancox, and A. Nabavizadeh. 2018. A redescription of the Triassic kannemeyeriiform dicynodont *Sangusaurus* (Therapsida, Anomodontia),

with an analysis of its feeding system. Journal of Vertebrate Paleontology 37:189–227.

Arbez, T., C. A. Sidor, and J. S. Steyer. 2018. *Laosuchus naga* gen. et sp. nov., a new chroniosuchian from South-East Asia (Laos) with internal structures revealed by micro-CT scan and discussion of its palaeobiology. Journal of Systematic Palaeontology: 10.1080/14772019.2018.1504827.

Battail, B. 2009. Late Permian dicynodont fauna from Laos. Geological Society, London, Special Publications 315:33–40.

Bernardi, M., F. M. Petti, and M. J. Benton. 2018. Tetrapod distribution and temperature rise during the Permian–Triassic mass extinction. Proceedings of the Royal Society B: Biological Sciences 285:20172331.

Bernardi, M., F. M. Petti, E. Kustatscher, M. Franz, C. Hartkopf-Fröder, C. C. Labandeira, T. Wappler, J. H. A. van Konijnenburg-van Cittert, B. R. Peecook, and K. D. Angielczyk. 2017. Late Permian (Lopingian) terrestrial ecosystems: A global comparison with new data from the low-latitude Bletterbach Biota. Earth-Science Reviews 175:18–43.

Benton, M. J., and A. J. Newell. 2014. Impacts of global warming on Permo–Triassic terrestrial ecosystems. Gondwana Research 25:1308–1337.

Benton, M. J., V. P. Tverdokhlebov, and M. V. Surkov. 2004. Ecosystem remodelling among vertebrates at the Permian–Triassic boundary in Russia. Nature 432:97–100.

Bercovici, A., S. Bourquin, J. Broutin, J. -S. Steyer, B. Battail, M. Véran, R. Vacant, B. Khenthavong, and S. Vongphamany. 2012. Permian continental paleoenvironments in Southeastern Asia: New insights from the Luang Prabang Basin (Laos). Journal of Asian Earth Sciences 60:197–211.

Blanchard, S., C. Rossignol, S. Bourquin, M. -P. Dabard, E. Hallot, T. Nalpas, M. Poujol, B. Battail, N. -E. Jalil, J.-S. Steyer, R. Vacant, M. Véran, A. Bercovici J. B. Diez, J. -L. Paquette, B. Khenthavong, and S. Vongphamany. 2013. Late Triassic volcanic activity in South-East Asia: New stratigraphical, geochronological and paleontological evidence from the Luang Prabang Basin (Laos). Journal of Asian Earth Sciences 70–71:8–26.

Boos, A. D. S., C. F. Kammerer, C. L. Schultz, M. B. Soares, and A. L. R. Ilha. 2016. A New Dicynodont (Therapsida: Anomodontia) from the Permian of Southern Brazil and Its Implications for Bidentalian Origins. PLoS One 11:e0155000.

Botha, J. and R. M. H. Smith. 2006. Rapid vertebrate recuperation in the Karoo Basin of South Africa following the End-Permian extinction. Journal of African Earth Sciences 45:502–514.

Botha-Brink, J., and K. D. Angielczyk. 2010. Do extraordinarily high growth rates in Permo–Triassic dicynodonts (Therapsida, Anomodontia) explain their success before and after the end-Permian extinction ? Zoological Journal of the Linnean Society 160:341–365.

Botha-Brink, J., D. Codron, A. K. Huttenlocker, K. D. Angielczyk, and M. Ruta. 2016. Breeding Young as a Survival Strategy during Earth's Greatest Mass Extinction. Scientific Reports 6:24053.

Bremer, K. 1988. The limits of amino acid sequence data in angiosperm phylogenetic reconstruction. Evolution 42:795–803.

Broom, R. 1905. On the use of the term Anomodontia. Albany Museum Records 1:266–269.

Buchwitz, M., F. Witzmann, S. Voigt, and V. Golubev. 2012. Osteoderm microstructure indicates the presence of a crocodylian-like trunk bracing system in a group of armoured basal tetrapods. Acta Zoologica 93:260–280.

Buffetaut, E. 1989. The contribution of vertebrate palaeontology to the geodynamic history of South East Asia; pp. 645–653 in A.M.C. Şengör (ed.), Tectonic Evolution of the Tethyan Region. Kluwer Academic Publishers, Dordrecht, Netherlands.

Burgess, S. D., S. A. Bowring, and S. -Z. Shen. 2014. High-precision timeline for Earth's most severe extinction. Proceedings of the National Academy of Sciences 111:3316–3321.

Burrett, C., K. Zaw, S. Meffre, C. K. Lai, S. Khositanont, P. Chaodumrong, M. Udchachon, S. Ekins, and J. Halpin. 2014. The configuration of Greater Gondwana—Evidence from LA ICPMS, U–Pb geochronology of detrital zircons from the Palaeozoic and Mesozoic of Southeast Asia and China. Gondwana Research 26:31–51.

Castanhinha, R., R. Araújo, L. C. Júnior, K. D. Angielczyk, G. G. Martins, R. M. S. Martins, C. Chaouiya, F. Beckmann, and F. Wilde. 2013. Bringing Dicynodonts Back to Life: Paleobiology and Anatomy of a New Emydopoid Genus from the Upper Permian of Mozambique. PLoS ONE 8:e80974.

Chang, K. -H., and X. Zhao. 2012. North and South China suturing in the east end: What happened in Korean Peninsula? Gondwana Research 22:493–506.

Chaodumrong, P., X. -D. Wang, and S. -Z. Shen. 2007. Permian lithostratigraphy of the Shan–Thai Terrane in Thailand: revision of the Kaeng Krachan and Ratburi groups; pp. 229–236 in GEOTHAI'07 International Conference on Geology of Thailand: Towards Sustainable Development and Sufficiency Economy, Bangkok.

Chen, Z. -Q., and M. J. Benton. 2012. The timing and pattern of biotic recovery following the end-Permian mass extinction. Nature Geoscience 5:375–383.

Cluver, M. A. 1971. The cranial morphology of the dicynodont genus *Lystrosaurus*. Annals of South African Museum 56:155–274.

Cluver, M. A., and N. Hotton III. 1981. The genera *Dicynodon* and *Diictodon* and their bearing of classification of the Dicynodontia (Reptilia, Therapsida). Annales of the South African Museum 83:99–146.

Cluver M. A., and G. M. King. 1983. A reassessment of the relationships of Permian Dicynodontia (Reptilia, Therapsida) and a new classification of dicynodonts. Annals of the South African Museum 91:195–273.

Cocks, L. R. M., and T. H. Torsvik. 2013. The dynamic evolution of the Palaeozoic geography of eastern Asia. Earth-Science Reviews 117:40–79.

Colbert, E. H. 1982. The distribution of *Lystrosaurus* in Pangaea and its implications. Geobios 15:375–383.

Counillon, H. 1896. Documents pour servir à l'étude géologique des environs de Luang–Prabang (Cochinchine). Comptes rendus de l'Académie des sciences 123:1330–1333.

Cox, C. B., and K. D. Angielczyk. 2015. A New Endothiodont Dicynodont (Therapsida, Anomodontia) from the Permian Ruhuhu Formation (Songea Group) of Tanzania and Its Feeding System. Journal of Vertebrate Paleontology 35:e935388.

Das Gupta, H. C. 1922. Notes on the Panchet Reptile; pp. 237–241, Sir Asutosh Mukherjee Silver Jubilee Volumes, Volume 2. University Press, Calcutta.

Dutuit, J. M. 1988. Ostéologie crânienne et ses enseignements, apports géologique et paléoécologique, de *Moghreberia nmachouensis*, Dicynodonte (Reptilia,

Therapsida) du Trias supérieur marocain. Bulletin du Muséum national d'histoire naturelle, Section C, Sciences de la terre, paléontologie, géologie, minéralogie 10:227–285.

Faure, M., C. Lepvrier, V. V. Nguyen, T. V. Vu, W. Lin, and Z. Chen. 2014. The South China block-Indochina collision: Where, when, and how? Journal of Asian Earth Sciences 79:260–274.

Fröbisch, J. 2007. The cranial anatomy of *Kombuisia frerensis* Hotton (Synapsida, Dicynodontia) and a new phylogeny of anomodont therapsids. Zoological Journal of the Linnean Society 150:117–144.

Fröbisch, J. 2008. Global Taxonomic Diversity of Anomodonts (Tetrapoda, Therapsida) and the Terrestrial Rock Record Across the Permian-Triassic Boundary. PLoS ONE 3:e3733.

Fröbisch, J. 2009. Composition and similarity of global anomodont-bearing tetrapod faunas. Earth-Science Reviews 95:119–157.

Fröbisch, J., K. D. Angielczyk, and C. A. Sidor. 2010. The Triassic dicynodont *Kombuisia* (Synapsida, Anomodontia) from Antarctica, a refuge from the terrestrial Permian-Triassic mass extinction. Naturwissenschaften 97:187–196.

Gastaldo, R. A., J. Neveling, C. V. Looy, M. K. Bamford, S. L. Kamo, and J. W. Geissman. 2017. Paleontology of the Blaauwater 67 and 65 farms, South Africa: testing the *Daptocephalus*/*Lystrosaurus* biozone boundary in a stratigraphic framework. Palaios 32:349–366.

Germain, D., and M. Laurin. 2005. Microanatomy of the radius and lifestyle in amniotes (Vertebrata, Tetrapoda). Zoologica Scripta 34:335–350.

Goloboff, P. A. 1999. Analyzing large data sets in reasonable times: solutions for composite optima. Cladistics 15:415–428.

Goloboff, P. A., C. I. Mattoni, and A. S. Quinteros. 2006. Continuous characters analyzed as such. Cladistics 22:589–601.

Goloboff, P. A., J. S. Farris, and K. C. Nixon. 2008. TNT, a free program for phylogenetic analysis. Cladistics 24:774–786.

Golubev, V. K. 2015. Dinocephalian stage in the history of the Permian tetrapod fauna of Eastern Europe. Paleontological Journal 49:1346–1352.

Green, J. L., M. H. Schweitzer, and E. -T. Lamm. 2010. Limb bone histology and growth in *Placerias hesternus* (Therapsida: Anomodontia) from the Upper Triassic of North America. Palaeontology 53:347–364.

Grine, F. E., C. A. Forster, M. A. Cluver, and J. A. Georgi. 2006. Cranial variability, ontogeny and taxonomy of *Lystrosaurus* from the Karoo Basin of South Africa; pp. 432–503 in Amniote Paleobiology: Perspectives on the Evolution of Mammals, Birds, and Reptiles, University of Chicago Press. Carrano M. T., Gaudin T. J., Blob R. W. & Wible J. R., Chicago.

Halpin, J. A., H. T. Tran, C. -K. Lai, S. Meffre, A. J. Crawford, and K. Zaw. 2016. U–Pb zircon geochronology and geochemistry from NE Vietnam: A “tectonically disputed” territory between the Indochina and South China blocks. Gondwana Research 34:254–273.

Kammerer, C. F., and K. D. Angielczyk. 2009. A proposed higher taxonomy of anomodont therapsids. Zootaxa 2018:1–24.

Kammerer, C. F., and R. M. H. Smith. 2017. An early geikiid dicynodont from the *Tropidostoma* Assemblage Zone (late Permian) of South Africa. PeerJ 5:e2913.

Kammerer, C. F., K. D. Angielczyk, and J. Fröbisch. 2011. A comprehensive taxonomic revision of “*Dicynodon*” (Therapsida, Anomodontia) and its implications

for dicynodont phylogeny, biogeography, and biostratigraphy. Journal of Vertebrate Paleontology 31:1–158.

Kammerer, C. F., J. Fröbisch, and K. D. Angielczyk. 2013. On the Validity and Phylogenetic Position of *Eubrachiosaurus browni*, a Kannemeyeriiform Dicynodont (Anomodontia) from Triassic North America. PLoS ONE 8:e64203.

Kammerer, C. F., K. D. Angielczyk, and J. Fröbisch. 2016. Redescription of the geikiid *Pelanomodon* (Therapsida, Dicynodontia), with a reconsideration of '*Propelanomodon*.' Journal of Vertebrate Paleontology 36:e1030408.

Kamvong, T., K. Zaw, S. Meffre, R. Maas, H. Stein, and C. -K. Lai. 2014. Adakites in the Truong Son and Loei fold belts, Thailand and Laos: Genesis and implications for geodynamics and metallogeny. Gondwana Research 26:165–184.

Keyser, A. W. 1969. A re-evaluation of the systematics and morphology of certain anomodont Therapsida. Ph.D. dissertation, University of the Witwatersrand, Johannesburg, South Africa, 325 pp.

Keyser, A. W., and A. R. I. Cruickshank. 1979. The origins and classification of Triassic dicynodonts. Transactions of the Geological Society of South Africa 82:81–108.

King, G. M. 1988. Anomodontia; pp. 1–174 in G. Fisher (ed.) Handbuch Der Paläoherpetologie, 17. G. Fischer Verlag, Stuttgart.

King, G. M., and M. A. Cluver. 1990. The aquatic *Lystrosaurus*: an alternative lifestyle. Historical Biology 4:323–341.

Kurkin, A. A. 2010. Late Permian dicynodonts of Eastern Europe. Paleontological Journal 44:672–681.

Lai, C.-K., S. Meffre, A. J. Crawford, K. Zaw, C.-D. Xue, and J. A. Halpin. 2014. The Western Ailaoshan Volcanic Belts and their SE Asia connection: A new tectonic model for the Eastern Indochina Block. Gondwana Research 26:52–74.

Lepvrier, C., H. Maluski, V. Van Tich, A. Leyreloup, P. Truong Thi, and N. Van Vuong. 2004. The Early Triassic Indosinian orogeny in Vietnam (Truong Son Belt and Kontum Massif); implications for the geodynamic evolution of Indochina. Tectonophysics, Asthenosphere-Lithosphere Dynamic Responses to Tethyan Plate Collisions 393:87–118.

Li, Z. -X. 1994. Collision between the North and South China blocks: a crustal-detachment model for suturing in the region east of the Tanlu fault. Geology 22:739–742.

Liu, J., M. -D. Tran, Y. Tang, Q. -L. Nguyen, T. -H. Tran, W. Wu, J. Chen, Z. Zhang, and Z. Zhao. 2012. Permo-Triassic granitoids in the northern part of the Truong Son belt, NW Vietnam: Geochronology, geochemistry and tectonic implications. Gondwana Research 22:628–644.

Liu, J., L. Li, and X.-W. Li. 2013. SHRIMP U–Pb zircon dating of the Triassic Ermaying and Tongchuan formations in Shanxi, China and its stratigraphic implications. Vertebrata Palasiatica 51:162–168.

Liu, J., J. Ramezani, L. Li, Q.-H. Shang, G.-H. Xu, Y.-Y. Wang, and J.-S. Yang. 2018. High-precision temporal calibration of Middle Triassic vertebrate biostratigraphy: U-Pb zircon constraints for the *Sinokannemeyeria* Fauna and Yonghesuchus. Vertebrata Palasiatica 56:16–24.

Lucas, S. G., and S. K. Harris. 1996. Taxonomic and biochronological significance of specimens of the Triassic dicynodont *Dinodontosaurus* Romer 1943 in the Tübingen collection. Paläontologische Zeitschrift 70:603–622.

Maisch, M. W. 2001. Observations on Karoo and Gondwana vertebrates. Part 2: A new skull-reconstruction of *Stahleckeria potens* von Huene, 1935 (Dicynodon, Middle Triassic) and a reconsideration of kannemeyeriiform phylogeny. Neues Jahrbuch für Geologie und Paläontologie Abhandlungen, 220:127–152.

Maisch, M. W. 2002. A new basal lystrosaurid dicynodont from the Upper Permian of South Africa. Palaeontology 45:343–359.

Maisch, M. W., and A. T. Matzke. 2014. *Sungeodon kimkraemerae* n. gen. n. sp., the oldest kannemeyeriiform (Therapsida, Dicynodontia) and its implications for the early diversification of large herbivores after the P/T boundary. Neues Jahrbuch für Geologie und Paläontologie 272:1–12.

Metcalfe, I. 2006. Palaeozoic and Mesozoic tectonic evolution and palaeogeography of East Asian crustal fragments: The Korean Peninsula in context. Gondwana Research 9: 24–46.

Metcalfe, I. 2011. Tectonic framework and Phanerozoic evolution of Sundaland. Gondwana Research 19:3–21.

Metcalfe, I. 2013. Gondwana dispersion and Asian accretion: Tectonic and palaeogeographic evolution of eastern Tethys. Journal of Asian Earth Sciences 66:1–33.

Nakano, N., Y. Osanai, N. T. Minh, T. Miyamoto, Y. Hayasaka, and M. Owada. 2008. Discovery of high-pressure granulite-facies metamorphism in northern Vietnam: Constraints on the Permo–Triassic Indochinese continental collision tectonics. Comptes Rendus Geoscience 340:127–138.

Olson, E. C. 1944. Origin of mammals based upon cranial morphology of the therapsid suborders. Geological Society of America Special Papers 55:1–136.

Owen, R. 1860. On the orders of fossil and recent Reptilia, and their distribution in time. Report of the Twenty-Ninth Meeting of the British Association for the Advancement of Science, 1859:153–166.

Piveteau, J. 1938. Un Therapside d'Indochine. Remarques sur la notion de continent de Gondwana. Annales de Paléontologie 27:137–152.

Racey, A. 2009. Mesozoic red bed sequences from SE Asia and the significance of the Khorat Group of NE Thailand. Geological Society, London, Special Publications 315:41–67.

Ray, S. 2005. *Lystrosaurus* (Therapsida, Dicynodontia) from India: Taxonomy, relative growth and Cranial dimorphism. Journal of Systematic Palaeontology 3:203–221.

Ray, S. 2006. Functional and evolutionary aspects of the postcranial anatomy of dicynodonts (Synapsida, Therapsida). Palaeontology 49:1263–1286.

Ray, S., A. Chinsamy, and S. Bandyopadhyay. 2005. *Lystrosaurus murrayi* (Therapsida, Dicynodontia): bone histology, growth and lifestyle adaptations. Palaeontology 48:1169–1185.

Ray, S., S. Bandyopadhyay, and R. Appana. 2010. Bone Histology of a Kannemeyeriid Dicynodont *Wadiasaurus*: Palaeobiological Implications; pp. 73–89 in S. Bandyopadhyay (ed.) New Aspects of Mesozoic Biodiversity. Springer, Heidelberg, Berlin.

Ray, S., J. Botha-Brink, and A. Chinsamy-Turan. 2012. Dicynodont growth dynamics and lifestyle adaptations; pp. 121–148 in A. Chinsamy-Turan (ed.) Forerunners of Mammals, Indiana University Press, Bloomington, Indiana.

Renaut, A. 2000. A re-evaluation of the cranial morphology and taxonomy of the Triassic dicynodont genus *Kannemeyeria*. Ph.D. dissertation, University of the Witwatersrand, Johannesburg, South Africa, 214 pp.

Renaut, A. J., R. J. Damiani, and P. J. Hancox. 2003. A taxonomic note concerning a dicynodont (Synapsida: Anomodontia) from the Middle Triassic of East Africa. 93–94.

Repelin, J. 1923. Sur un fragment de crâne de *Dicynodon*, recueilli par H. Counillon dans les environs de Luang-Prabang (Haut-Laos). Bulletin du Service Géologique de l'Indochine 12:1–7.

Rossignol, C., S. Bourquin, M. Poujol, E. Hallot, M. -P. Dabard, and T. Nalpas. 2016. The volcaniclastic series from the Luang Prabang Basin, Laos: A witness of a triassic magmatic arc? Journal of Asian Earth Sciences 120:159–183.

Rossignol, C., S. Bourquin, E. Hallot, M. Poujol, M.-P. Dabard, R. Martini, M. Villeneuve, J.-J. Cornée, A. Brayard, and F. Roger. 2018. The Indosinian orogeny: A perspective from sedimentary archives of north Vietnam. Journal of Asian Earth Sciences 158:352–380.

Sahney, S., and M. J. Benton. 2008. Recovery from the most profound mass extinction of all time. Proceedings of the Royal Society of London B: Biological Sciences 275:759–765.

Saurin, E. 1962. Luang Prabang Est. Carte géologique du Vietnam, Cambodge, Laos 1:500,000. Service géographique national, Dalat, Vietnam.

Scotese, C. R. 2014. Atlas of Middle & Late Permian and Triassic Paleogeographic Maps: Early Triassic. Paleomap Project, Department of Geology, University of Texas at Arlington. Available at www.scotese.com. Accessed March 9, 2017.

Shen, S. -Z., H. Zhang, G. R. Shi, W. Li, J. Xie, L. Mu, and J. Fan. 2013. Early Permian (Cisuralian) global brachiopod palaeobiogeography. Gondwana Research 24:104–124.

Smith, R. M. H., and J. Botha-Brink. 2014. Anatomy of a mass extinction: Sedimentological and taphonomic evidence for drought-induced die-offs at the Permo-Triassic boundary in the main Karoo Basin, South Africa. Palaeogeography, Palaeoclimatology, Palaeoecology 396:99–118.

Steyer, J. -S. 2009. The geological and palaeontological exploration of Laos; following in the footsteps of J. B. H. Counillon and A. Pavie. Geological Society, London, Special Publications 315:25–32.

Steyer, J. -S. (ed.). 2012. Earth before the dinosaurs. Indiana University Press, Bloomington, 182 pp.

Strong, E. E., and D. Lipscomb. 1999. Character Coding and Inapplicable Data. Cladistics 15:363–371.

Sullivan, C., R. R. Reisz, and R. M. H. Smith. 2003. The Permian mammal-like herbivore *Diictodon*, the oldest known example of sexually dimorphic armament. Proceedings of the Royal Society of London B: Biological Sciences 270:173–178.

Sun, Y., M. M. Joachimski, P. B. Wignall, C. Yan, Y. Chen, H. Jiang, L. Wang, and X. Lai. 2012. Lethally Hot Temperatures During the Early Triassic Greenhouse. Science 338:366–370.

Surkov, M. V., and M. J. Benton. 2004. The basicranium of dicynodonts (Synapsida) and its use in phylogenetic analysis. Palaeontology 47:619–638.

Thanh, N. X., M. T. Tu, T. Itaya, and S. Kwon. 2011. Chromian-spinel compositions from the Bo Xinh ultramafics, Northern Vietnam: Implications on tectonic evolution

of the Indochina block. Journal of Asian Earth Sciences, Suture Zones and Geodynamic Processes Suture Zones and Geodynamic Processes 42:258–267.

Tollman, S. M., F. E. Grine, and B. D. Hahn. 1980. Ontogeny and sexual dimorphism in *Aulacephalodon* (Reptilia, Anomodontia). Annals of the South Afncan Museum 8:159–186.

Torsvik, T. H., and J. R. M. Cocks (eds). 2017. Earth history and palaeogeography. Cambridge University Press, University of Cambridge, Cambridge, 332 pp.

Ueno, K. 2003. The Permian fusulinoidean faunas of the Sibumasu and Baoshan blocks: their implications for the paleogeographic and paleoclimatologic reconstruction of the Cimmerian Continent. Palaeogeography, Palaeoclimatology, Palaeoecology 193:1–24.

Viglietti, P. A., R. M. H. Smith, and B. S. Rubidge. 2018. Changing palaeoenvironments and tetrapod populations in the *Daptocephalus* Assemblage Zone (Karoo Basin, South Africa) indicate early onset of the Permo-Triassic mass extinction. Journal of African Earth Sciences 138:102–111.

Vượng, N. V., B. T. Hansen, K. Wemmer, C. Lepvrier, V. Tích, and T. Trọng Thắng. 2013. U/Pb and Sm/Nd dating on ophiolitic rocks of the Song Ma suture zone (northern Vietnam): Evidence for upper paleozoic paleotethyan lithospheric remnants. Journal of Geodynamics 69:140–147.

Wall, W. P. 1983. The correlation between high limb-bone density and aquatic habits in recent mammals. Journal of Paleontology 57:197–207.

Wang, X. -D., and T. Sugiyama. 2002. Permian coral faunas of the eastern Cimmerian Continent and their biogeographical implications. Journal of Asian Earth Sciences, Permian of Southeast Asia 20:589–597.

Wang, X. –D., W. Lin, S. -Z. Shen, P. Chaodumrong, G. R. Shi, X. Wang, and Q. Wang. 2013. Early Permian rugose coral *Cyathaxonia* faunas from the Sibumasu Terrane (Southeast Asia) and the southern Sydney Basin (Southeast Australia): Paleontology and paleobiogeography. Gondwana Research 24:185–191.

Ward, P. D., J. Botha, R. Buick, M. O. De Kock, D. H. Erwin, G. H. Garrison, J. L. Kirschvink, and R. M. H. Smith. 2005. Abrupt and Gradual Extinction Among Late Permian Land Vertebrates in the Karoo Basin, South Africa. Science 307:709–714.

Weislogel, A. L., S. A. Graham, E. Z. Chang, J. L. Wooden, G. E. Gehrels, and H. Yang. 2006. Detrital zircon provenance of the Late Triassic Songpan-Ganzi complex: Sedimentary record of collision of the North and South China blocks. Geology 34:97.

Wilmsen, M., F. T. Fürsich, K. Seyed-Emami, M. R. Majidifard, and J. Taheri. 2009. The Cimmerian Orogeny in northern Iran: tectono-stratigraphic evidence from the foreland. Terra Nova 21:211–218.

Woodward, A. S. 1932. Dicynodontidae; pp. 257–260 in K.A. Von Zittel (ed.) Textbook of Palaeontology. Macmillan, London.

Xiong, C., and Q. Wang. 2011. Permian–Triassic land-plant diversity in South China: Was there a mass extinction at the Permian/Triassic boundary? Paleobiology 37:157–167.

Yu, J. X., J. Broutin, Z. -Q Chen, X. Shi, H. Li, D. Chu, and Q. Huang. 2015. Vegetation changeover across the Permian–Triassic Boundary in Southwest China: Extinction, survival, recovery and palaeoclimate: A critical review. Earth-Science Reviews 149:203–224.

Yuan, P. L., and C. C. Young. 1934. On the Occurrence of *Lystrosaurus* in Sinkiang. Bulletin of the Geological Society of China 12:575–580.

Zanchi, A., S. Zanchetta, F. Berra, M. Mattei, E. Garzanti, S. Molyneux, A. Nawab, and J. Sabouri. 2009. The Eo-Cimmerian (Late? Triassic) orogeny in North Iran. Geological Society, Special Publications 312:31–55.

Zanchi, A., N. Malaspina, S. Zanchetta, F. Berra, L. Benciolini, M. Bergomi, A. Cavallo, H. R. Javadi, and M. Kouhpeyma. 2015. The Cimmerian accretionary wedge of Anarak, Central Iran. Journal of Asian Earth Sciences 102:45–72.

Zhang, R. Y., C. -H. Lo, S. -L Chung, M. Grove, S. Omori, Y. Iizuka, J. G. Liou, and T. Van Tri. 2013. Origin and Tectonic Implication of Ophiolite and Eclogite in the Song Ma Suture Zone between the South China and Indochina Blocks. Journal of Metamorphic Geology 31:49–62.

Zhang, R. Y., C. -H. Lo, X. -H. Li, S. -L Chung, T. T. Anh, and T. Van Tri. 2014. U-Pb dating and tectonic implication of ophiolite and metabasite from the Song Ma suture zone, northern Vietnam. American Journal of Science 314:649–678.

Submitted May 18, 2017; accepted Month DD, YYYY

FIGURE AND TABLE CAPTIONS

Figures

FIGURE 1. Continental blocks of Southeast Asia and geological map of the Luang Prabang Basin. **A**, Tectonic subdivisions of Southeast Asia after Metcalfe (2011); **B**, geological map of the Luang Prabang Basin with the emplacement of fossil sites and dated samples (modified after Blanchard et al., 2013). Sample LP03 was collected at

the dicynodont site, sample LP04 in an unfossiliferous site, and sample LP05 at the chroniosuchian site (Arbez et al., 2018). **Abbreviations**: **AL**, Ailaoshan suture zone; **CM**, Changning Menglian suture zone; **JH**, Jinghong suture zone; **NU**, Nan Uttaradit suture zone; **SK**, Sra Kaeo suture zone; **LP**, emplacement of the Luang Prabang Basin. [Intended for 2/3 of a whole page width]

FIGURE 2. Photographs and interpretive drawings of LPB 1993-3, the holotype of *Counillonia superoculis* gen. et sp. nov. Skull in **A**, dorsal; **B**, right lateral; **C**, ventral; and **D**, occipital views. The thin grey lines represent the sutures and the bold black ones represent the relief. The dotted line represents our interpretation of sutures based on variation in bone texture. Scale bar equals 5 cm. [Intended for whole page width]

FIGURE 3. Photographs and interpretive drawings of LPB 1993-2, the holotype of *Repelinosaurus robustus* gen. et sp. nov. Skull in **A**, dorsal; **B**, right lateral; **C**, ventral; and **D**, occipital views. The thin grey lines represent the sutures and the bold black ones represent the relief. Scale bar equals 5 cm. [Intended for whole page width]

FIGURE 4. Photographs and interpretive drawings of LPB 1995-9, a skull referred to *Repelinosaurus robustus* gen. et sp. nov. Skull in **A**, dorsal; **B**, right lateral; **C**, ventral; and **D**, occipital views. The thin grey lines represent the sutures and the bold black ones represent the relief. The dotted line represents our interpretation of sutures based on variation in bone texture. Scale bar equals 5 cm. [Intended for whole page width]

FIGURE 5. Close-up photograph and interpretive drawing of the lateral snout region of the referred skull LPB 1995-9, attributed to *Repelinosaurus robustus* gen. et sp. nov. The thin grey lines represent the sutures, and the bold black ones represent the relief. Scale bar equals 5 cm. [Intended for 2/3 of a whole page width]

FIGURE 6. The most parsimonious cladogram (1156.346 steps, CI = 0.236, RI = 0.712). Numbers at nodes represent the Bremer supports. Capital letters indicate the following clades (Maisch, 2001; Kammerer and Angielczyk, 2009): A, Dicynodontia. B, Pylaecephalidae. C, Endothiodontia. D, Therochelonia. E, Emydopoidea. F, Emydopidae. G, Kistecephalia. H, Kingoriidae. I, Cistecephalidae. J, Bidentalia. K, Cryptodontia. L, Rhachiocephalidae. M, Geikiidae. N, Geikiinae. O, Lystrosauridae. P, Kannemeyeriiformes. Q, Shansiodontidae. R, Stahleckeriidae. S, Kannemeyeriidae. [Intended for whole page width]

Tables

TABLE 1. Summary of the maximum depositional ages obtained by U–Pb Laser Ablation – Inductively Coupled – Mass Spectrometry dating on detrital zircon grains from volcaniclastic rocks of the samples collected in the Purple Claystone Formation (LP03, LP04, LP05) (Rossignol et al., 2016). LP03 was collected at the dicynodont fossil site. The MSWD and the probability given for the concordia ages are for both concordance and equivalence. **Abbreviations**: **MSWD**, mean square of weighted deviates; **n**, number of analyses used to calculate the maximum depositional age; **N**, number of concordant zircon grain; $\mathbf{N_a}$, number of analyses per sample; $\mathbf{N_{zr}}$, number of zircon grains analyzed per sample.

TABLE 2. Cranial measurements (in cm, scaled with Image J 1.50i) of the three Laotian dicynodont skulls attributed to *Counillonia superoculis* and *Repelinosaurus robustus*.

Appendices

APPENDIX 1. Continuous and discrete codings in the Laotian dicynodonts used in the phylogenetic analysis. The whole character-taxon matrix is available online as Supplementary Data 1.

Supplementary Data

SUPPLEMENTARY DATA 1. Data matrix used in the phylogenetic analysis (modified from Angielczyk and Kammerer, 2017) (Matrix.txt).

SUPPLEMENTARY DATA 2. List of characters (continuous and discrete) used in the phylogenetic analysis (modified from Angielczyk and Kammerer, 2017).

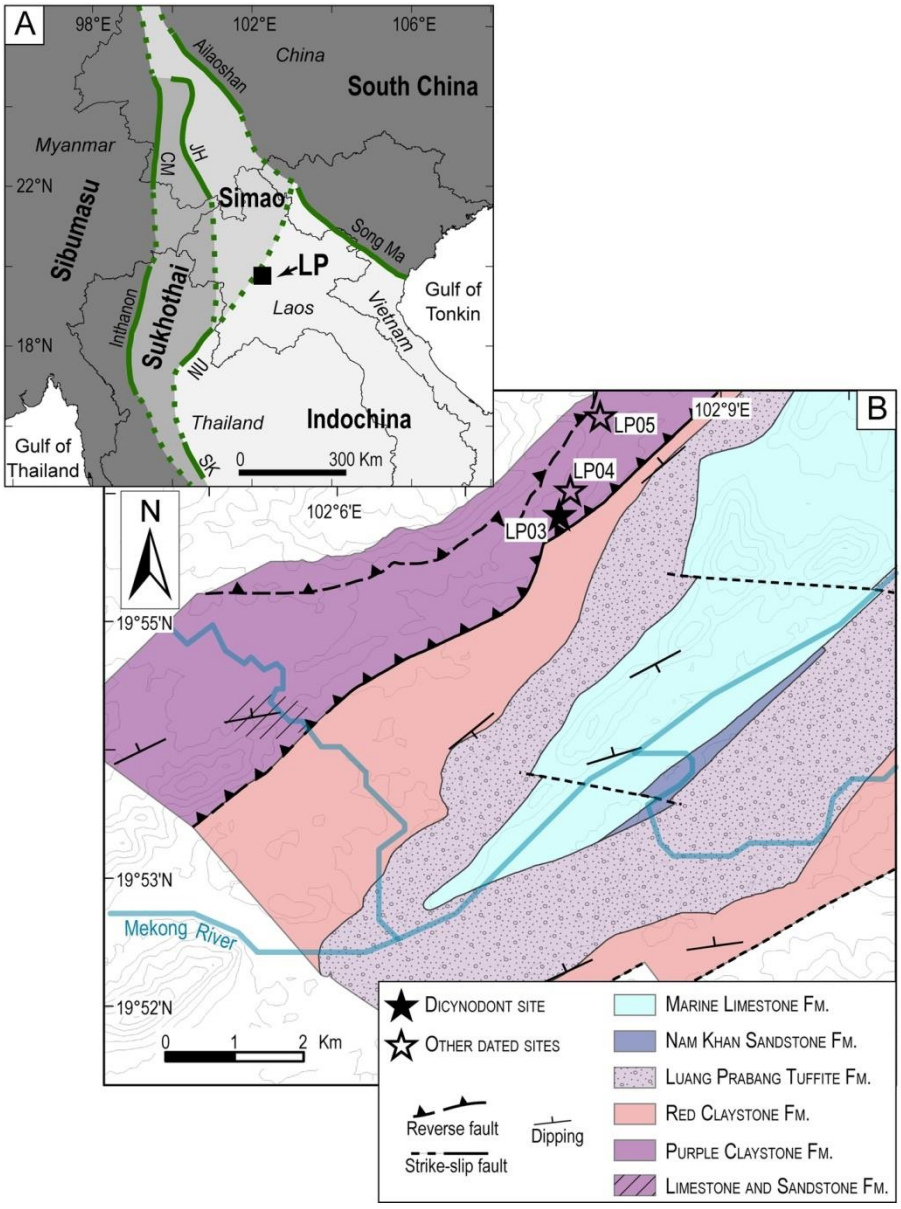

FIGURE 1. Continental blocks of Southeast Asia and geological map of the Luang Prabang Basin. **A**, Tectonic subdivisions of Southeast Asia after Metcalfe (2011); **B**, geological map of the Luang Prabang Basin with the emplacement of fossil sites and dated samples (modified after Blanchard et al., 2013). Sample LP03 was collected at the dicynodont site, sample LP04 in an unfossiliferous site, and sample LP05 at the chroniosuchian site (Arbez et al., 2018). **Abbreviations**: **AL**, Ailaoshan suture zone; **CM**, Changning Menglian suture zone; **JH**, Jinghong suture zone; **NU**, Nan Uttaradit suture zone; **SK**, Sra Kaeo suture zone; **LP**, emplacement of the Luang Prabang Basin. [Intended for 2/3 of a whole page width]

120x160mm (300 x 300 DPI)

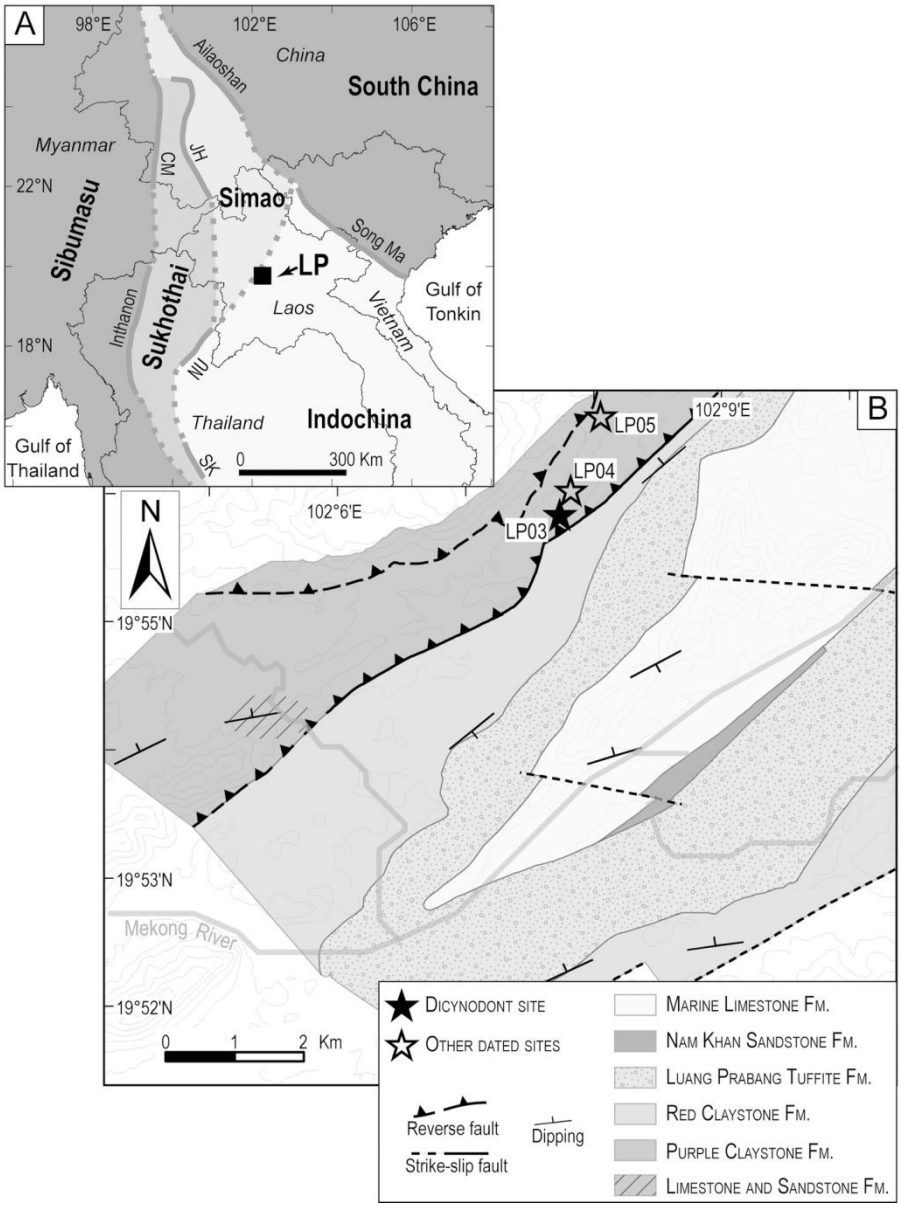

FIGURE 1. Continental blocks of Southeast Asia and geological map of the Luang Prabang Basin. **A**, Tectonic subdivisions of Southeast Asia after Metcalfe (2011); **B**, geological map of the Luang Prabang Basin with the emplacement of fossil sites and dated samples (modified after Blanchard et al., 2013). Sample LP03 was collected at the dicynodont site, sample LP04 in an unfossiliferous site, and sample LP05 at the chroniosuchian site (Arbez et al., 2018). **Abbreviations**: **AL**, Ailaoshan suture zone; **CM**, Changning Menglian suture zone; **JH**, Jinghong suture zone; **NU**, Nan Uttaradit suture zone; **SK**, Sra Kaeo suture zone; **LP**, emplacement of the Luang Prabang Basin. [Intended for 2/3 of a whole page width]

120x160mm (300 x 300 DPI)

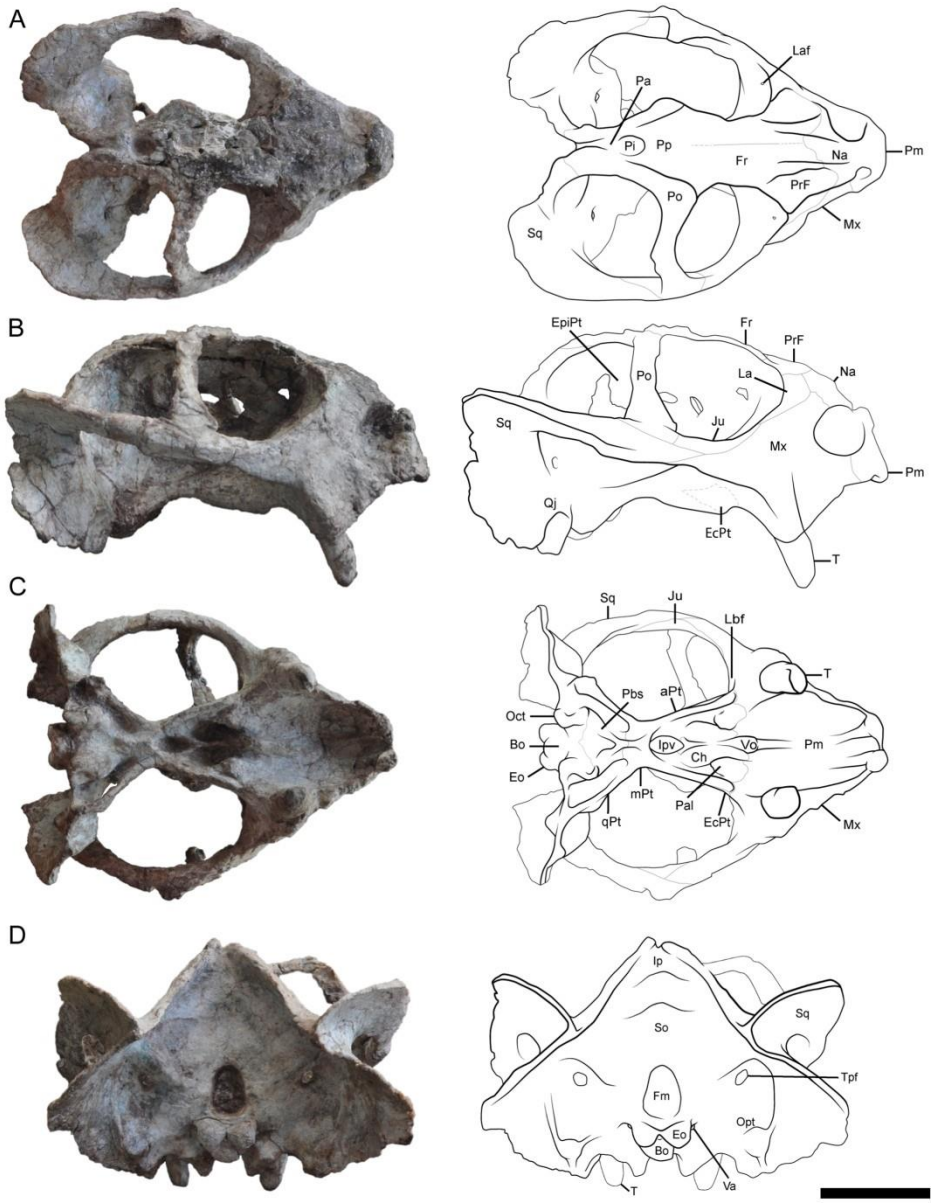

FIGURE 2. Photographs and interpretive drawings of LPB 1993-3, the holotype of *Counillonia superoculis* gen. et sp. nov. Skull in **A**, dorsal; **B**, right lateral; **C**, ventral; and **D**, occipital views. The thin grey lines represent the sutures and the bold black ones represent the relief. The dotted line represents our interpretation of sutures based on variation in bone texture. Scale bar equals 5 cm. [Intended for whole page width]

182x232mm (300 x 300 DPI)

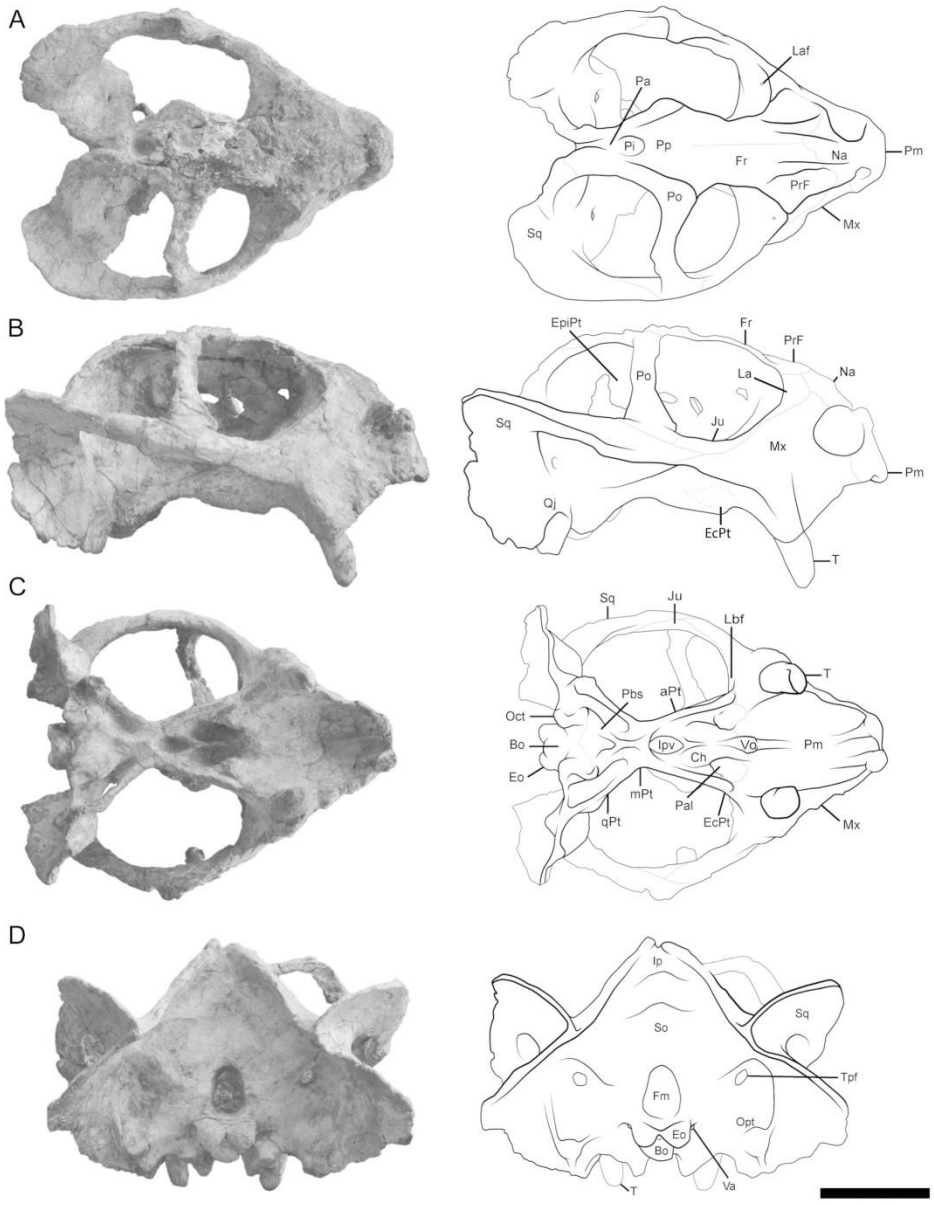

FIGURE 2. Photographs and interpretive drawings of LPB 1993-3, the holotype of *Counillonia superoculis* gen. et sp. nov. Skull in **A**, dorsal; **B**, right lateral; **C**, ventral; and **D**, occipital views. The thin grey lines represent the sutures and the bold black ones represent the relief. The dotted line represents our interpretation of sutures based on variation in bone texture. Scale bar equals 5 cm. [Intended for whole page width]

182x234mm (300 x 300 DPI)

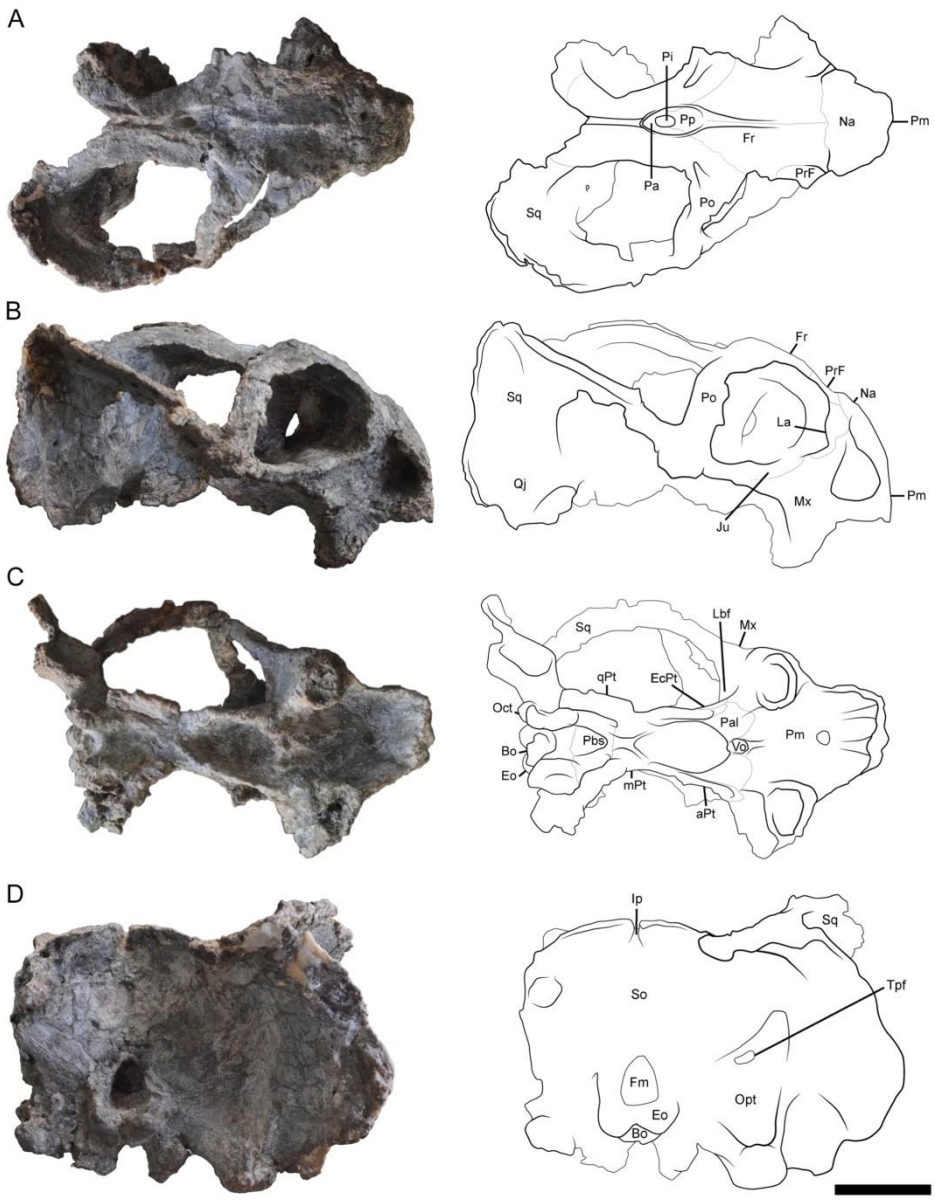

FIGURE 3. Photographs and interpretive drawings of LPB 1993-2, the holotype of *Repelinosaurus robustus* gen. et sp. nov. Skull in **A**, dorsal; **B**, right lateral; **C**, ventral; and **D**, occipital views. The thin grey lines represent the sutures and the bold black ones represent the relief. Scale bar equals 5 cm. [Intended for whole page width]

182x232mm (300 x 300 DPI)

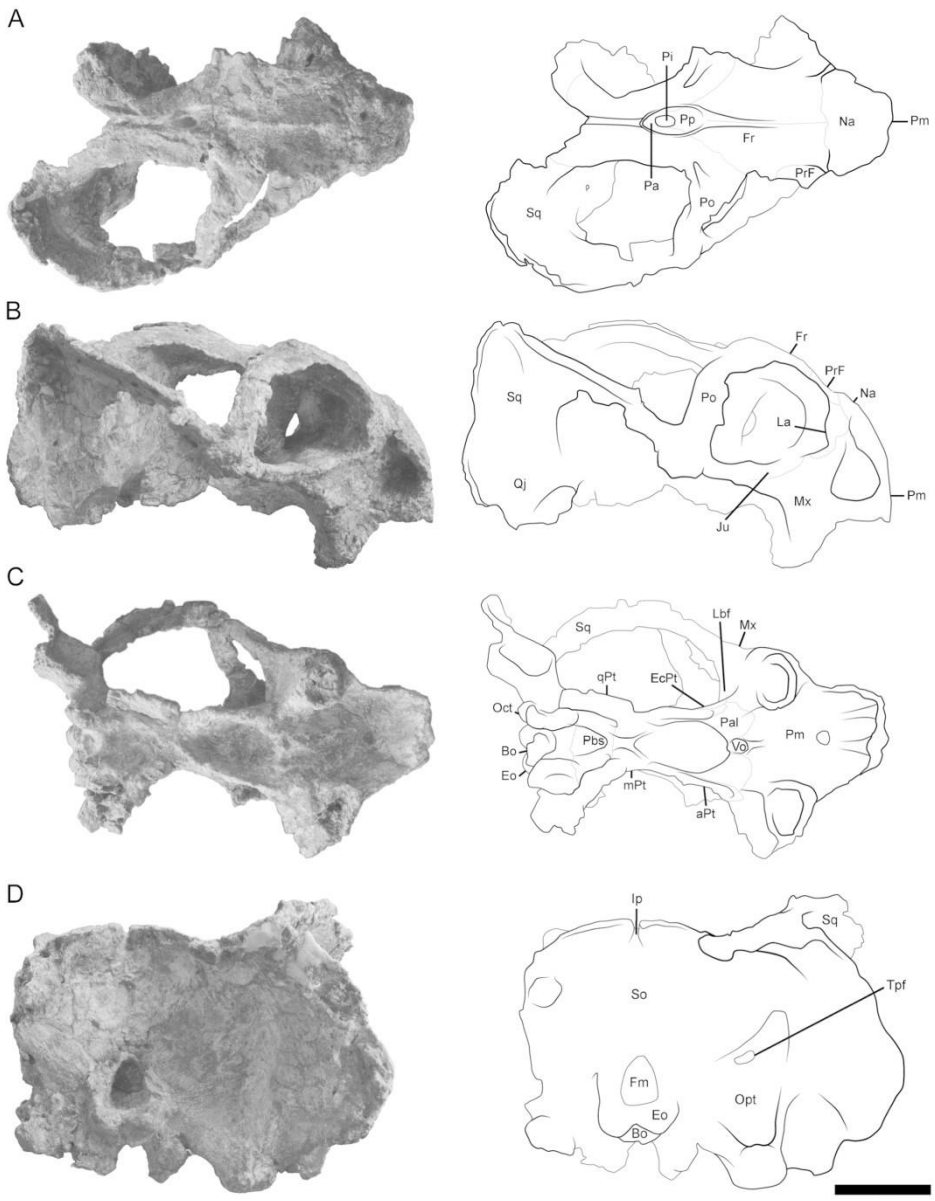

FIGURE 3. Photographs and interpretive drawings of LPB 1993-2, the holotype of *Repelinosaurus robustus* gen. et sp. nov. Skull in **A**, dorsal; **B**, right lateral; **C**, ventral; and **D**, occipital views. The thin grey lines represent the sutures and the bold black ones represent the relief. Scale bar equals 5 cm. [Intended for whole page width]

182x232mm (300 x 300 DPI)

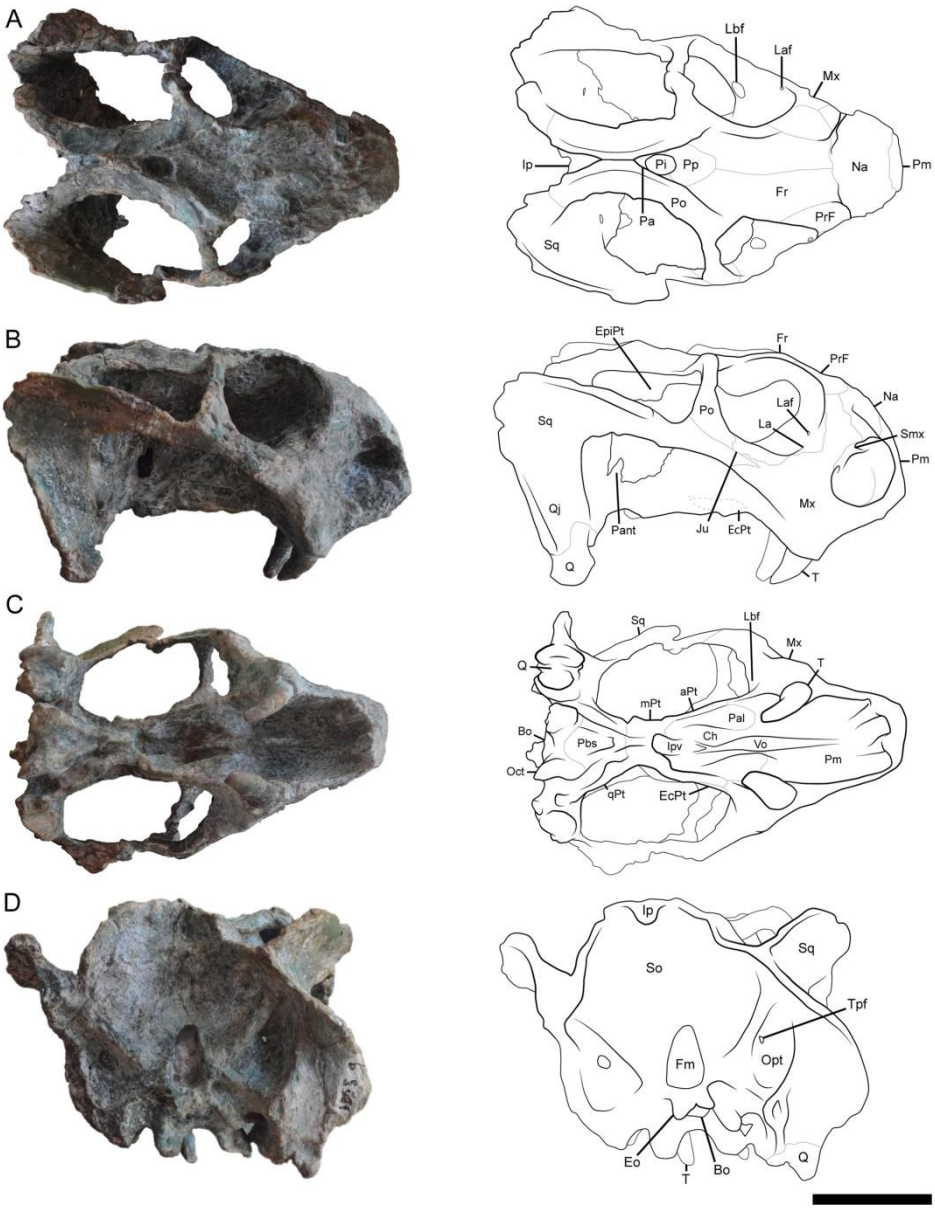

FIGURE 4. Photographs and interpretive drawings of LPB 1995-9, a skull referred to *Repelinosaurus robustus* gen. et sp. nov. Skull in **A**, dorsal; **B**, right lateral; **C**, ventral; and **D**, occipital views. The thin grey lines represent the sutures and the bold black ones represent the relief. The dotted line represents our interpretation of sutures based on variation in bone texture. Scale bar equals 5 cm. [Intended for whole page width]

182x230mm (300 x 300 DPI)

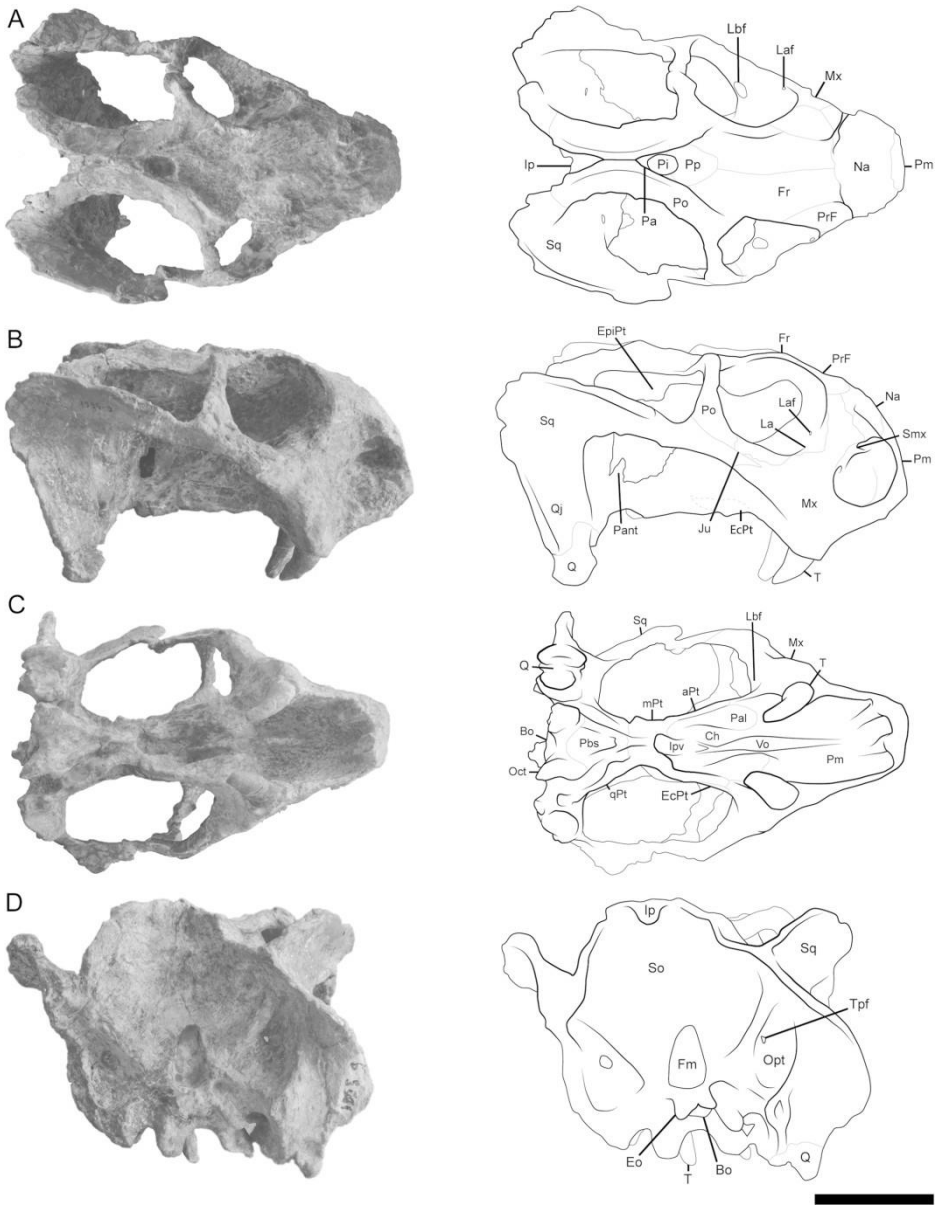

FIGURE 4. Photographs and interpretive drawings of LPB 1995-9, a skull referred to *Repelinosaurus robustus* gen. et sp. nov. Skull in **A**, dorsal; **B**, right lateral; **C**, ventral; and **D**, occipital views. The thin grey lines represent the sutures and the bold black ones represent the relief. The dotted line represents our interpretation of sutures based on variation in bone texture. Scale bar equals 5 cm. [Intended for whole page width]

182x230mm (300 x 300 DPI)

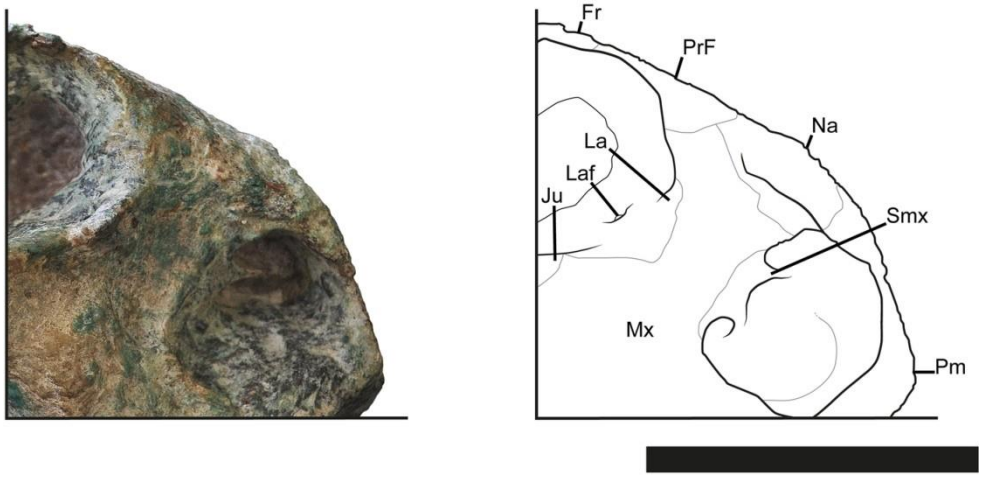

FIGURE 5. Close-up photograph and interpretive drawing of the lateral snout region of the referred skull LPB 1995-9, attributed to *Repelinosaurus robustus* gen. et sp. nov. The thin grey lines represent the sutures, and the bold black ones represent the relief. Scale bar equals 5 cm. [Intended for 2/3 of a whole page width]

120x61mm (300 x 300 DPI)

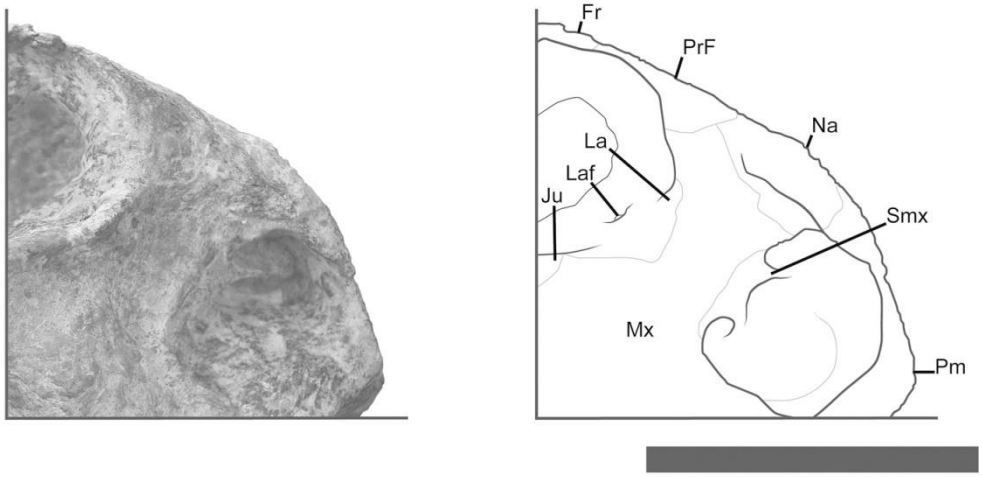

FIGURE 5. Close-up photograph and interpretive drawing of the lateral snout region of the referred skull LPB 1995-9, attributed to *Repelinosaurus robustus* gen. et sp. nov. The thin grey lines represent the sutures, and the bold black ones represent the relief. Scale bar equals 5 cm. [Intended for 2/3 of a whole page width]

120x61mm (300 x 300 DPI)

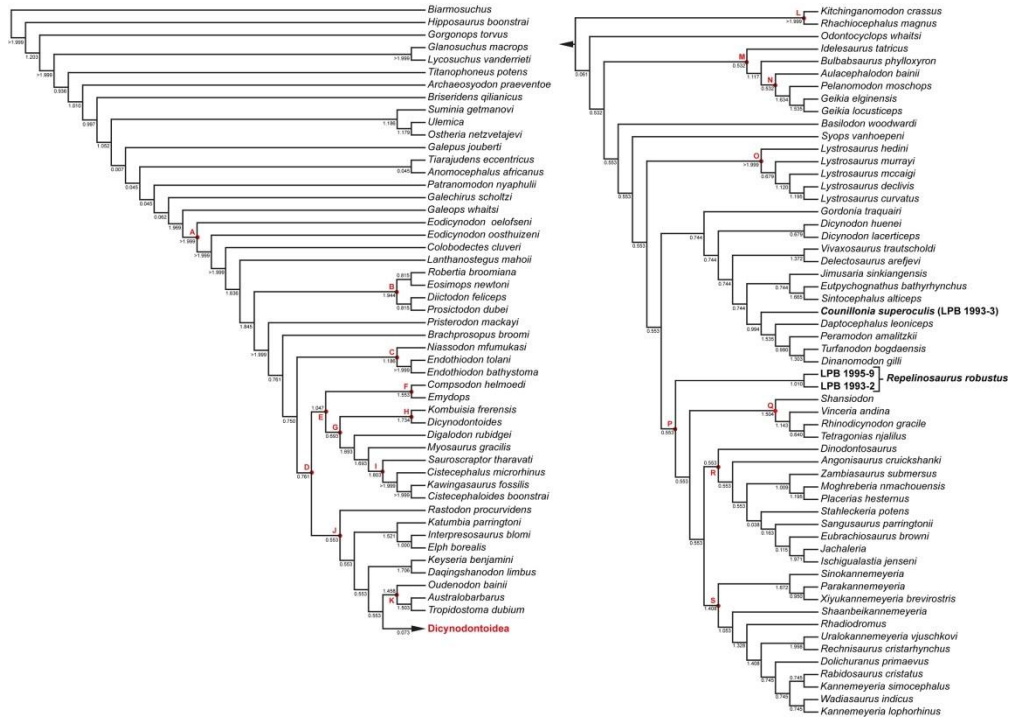

FIGURE 6. The most parsimonious cladogram (1156.346 steps, CI = 0.236, RI = 0.712). Numbers at nodes represent the Bremer supports. Capital letters indicate the following clades (Maisch, 2001; Kammerer and Angielczyk, 2009): A, Dicynodontia. B, Pylaecephalidae. C, Endothiodontia. D, Therochelonia. E, Emydopoidea. F, Emydopidae. G, Kistecephalia. H, Kingoriidae. I, Cistecephalidae. J, Bidentalia. K, Cryptodontia. L, Rhachiocephalidae. M, Geikiidae. N, Geikiinae. O, Lystrosauridae. P, Kannemeyeriiformes. Q, Shansiodontidae. R, Stahleckeriidae. S, Kannemeyeriidae. [Intended for whole page width]

233x182mm (300 x 300 DPI)

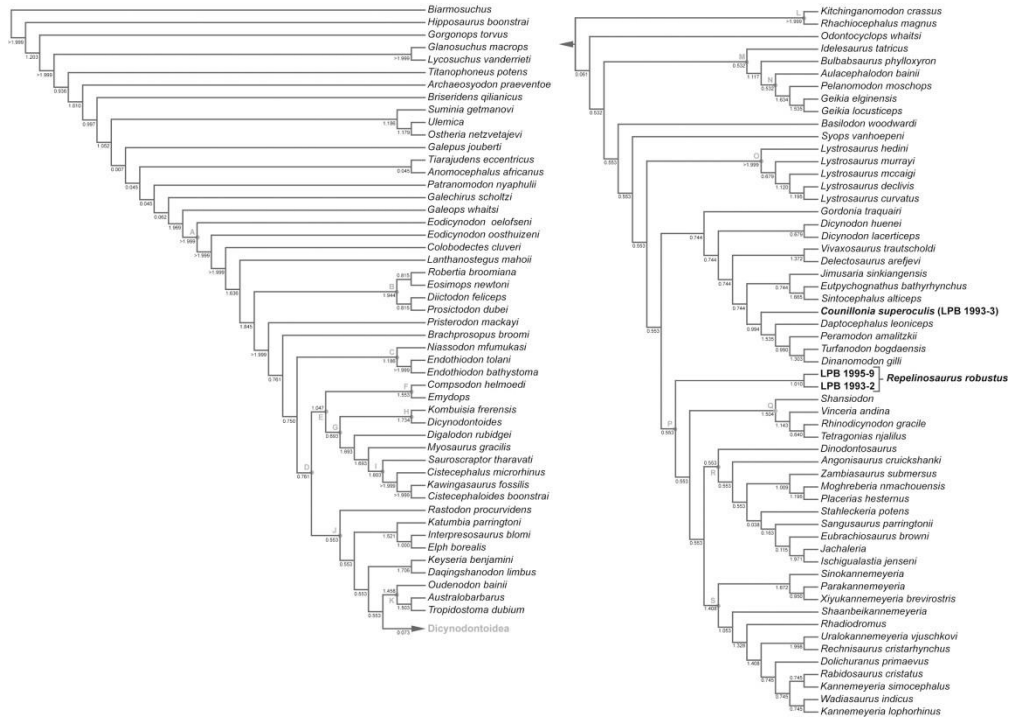

FIGURE 6. The most parsimonious cladogram (1156.346 steps, CI = 0.236, RI = 0.712). Numbers at nodes represent the Bremer supports. Capital letters indicate the following clades (Maisch, 2001; Kammerer and Angielczyk, 2009): A, Dicynodontia. B, Pylaecephalidae. C, Endothiodontia. D, Therochelonia. E, Emydopoidea. F, Emydopidae. G, Kistecephalia. H, Kingoriidae. I, Cistecephalidae. J, Bidentalia. K, Cryptodontia. L, Rhachiocephalidae. M, Geikiidae. N, Geikiinae. O, Lystrosauridae. P, Kannemeyeriiformes. Q, Shansiodontidae. R, Stahleckeriidae. S, Kannemeyeriidae. [Intended for whole page width]

233x182mm (300 x 300 DPI)

TABLE 1. Summary of the maximum depositional ages obtained by U–Pb Laser Ablation – Inductively Coupled – Mass Spectrometry dating on detrital zircon grains from volcaniclastic rocks of the samples collected in the Purple Claystone Formation (LP03, LP04, LP05) (Rossignol et al., 2016). LP03 was collected at the dicynodont fossil site. The MSWD and the probability given for the concordia ages are for both concordance and equivalence. **Abbreviations**: **MSWD**, mean square of weighted deviates; **n**, number of analyses used to calculate the maximum depositional age; **N**, number of concordant zircon grain; $\mathbf{N_a}$, number of analyses per sample; $\mathbf{N_{zr}}$, number of zircon grains analyzed per sample.

	N_a	N_{zr}	N	Maximum depositional age				
				Concordia age	± (2σ)	n	MSWD	Probability
LP03	105	102	25	252.0	2.6	6	0.89	0.55
LP04	41	36	7	300.5	3.7	4	0.73	0.65
LP05	96	95	39	251.0	1.4	21	0.55	0.99

TABLE 2. Cranial measurements (in cm, scaled with Image J 1.50i) of the three Laotian dicynodont skulls attributed to *Counillonia superoculis* and *Repelinosaurus robustus*.

	C. superoculis	*R. robustus*	
	LPB 1993-3	LPB 1995-9	LPB 1993-2
Basal length (from the tip of snout to the occipital condyle, in ventral view)	16.02	15.72	19.00
Maximum width (in dorsal view)	13.41	NA	NA
Maximum orbital height (in lateral view)	4.82	4.19	5.79
Maximum orbital length (in lateral view)	5.67	4.73	6.82
Mediolateral diameter of the tusk root (in ventral view)	1.27	1.46	2.02
Anteroposterior diameter of the tusk root (in ventral view)	1.56	0.90	1.49
Pineal foramen length (in dorsal view)	1.36	1.33	0.96
Pineal foramen width (in dorsal view)	0.96	0.87	0.66

APPENDIX 1. Continuous and discrete codings in the Laotian dicynodonts used in the phylogenetic analysis; en dash (–) indicates missing values. The whole character-taxon matrix is available online as Supplementary Data 1.

Continuous codings (characters 1 to 23)

LPB 1993-3 (holotype of to *Counillonia superoculis*)

0.2975.068 – – 0.276 0.134 – 0.131 8.333 0.140 – 9.616 0.876 – – – – – – – – – – –

LPB 1993-2 (holotype of *Repelinosaurus robustus*)

0.200 – 0.295 – 0.408 0.281 – – – – – 14.698 0.829 – – – – – – – – – – –

LPB 1995-9 (attributed to *Repelinosaurus robustus*)

0.205 – 0.254 – – 0.316 – 0.124 – 0.101 – – 0.935 – – – – – – – – – – –

Discrete codings (characters 24 to 194)

LPB 1993-3 (holotype of *Counillonia superoculis*)

1200221210100??00022??1101000??2????????0???????0?01002110020l1?0??111112103??1012101021l0?022?120????01011???

LPB 1993-2(holotype of *Repelinosaurus robustus*)

1200221210?10000?100?22??1101001?100?10??100201110000010021100201??0??????1????????1012??10?11??022?120????01??1???

APPENDIX 1. (Continued)

LPB 1995-9(attributed to *Repelinosaurus robustus*)

12002012101?000??100022??0101001?1000100l?0010?1100000100211?02??1?0

??11111210 30???1012101?2110?02???20????????1??????????????????????

????????????????????????????????????